Contribution of the Runx1 transcription factor to axonal pathfinding and muscle innervation by hypoglossal motoneurons

doi: 10.1002/dneu.22285

Contribution of the Runx1 transcription factor to axonal pathfinding and muscle innervation by hypoglossal motoneurons

Masaaki Yoshikawa[1, 2 †], Mizuki Hirabayashi[2 †], Ryota Ito[2 †], Shigeru Ozaki[2], Shin Aizawa[1], Tomoyuki Masuda[2], Kouji Senzaki[2], Takashi Shiga[2 *]

[1]Division of Anatomical Science, Department of Functional Morphology, Nihon University School of Medicine, 30-1 Oyaguchi-Kamicho, Itabashi, Tokyo 173-8610, Japan

[2]Doctoral Program in Kansei, Behavioral and Brain Sciences, Graduate School of Comprehensive Human Sciences, University of Tsukuba, 1-1-1 Tennodai, Tsukuba, Ibaraki 305-8577, Japan

[†]These three authors contributed equally.

*Corresponding author

Takashi Shiga, above address,

Phone and Fax number: +81-298-53-6960

E-mail: tshiga@md.tsukuba.ac.jp

34 text pages with 9 figures and 3 supplemental figures

Running title: Runx1 in hypoglossal axonal projections

Keywords: Runx, transcription factor, hypoglossal neuron, CGRP, axonal projection

ABSTRACT

The runt-related transcription factor Runx1 contributes to cell type specification and axonal targeting projections of the nociceptive dorsal root ganglion neurons. Runx1 is also expressed in the central nervous system, but little is known of its functions in brain development. At mouse embryonic day (E) 17.5, Runx1-positive neurons were detected in the ventrocaudal subdivision of the hypoglossal nucleus. Runx1-positive neurons lacked calcitonin gene-related peptide (CGRP) expression, whereas Runx1-negative neurons expressed CGRP. Expression of CGRP was not changed in *Runx1*-deficient mice at E17.5, suggesting that Runx1 alone does not suppress CGRP expression. Hypoglossal axon projections to the intrinsic vertical (V) and transverse (T) tongue muscles were sparser in *Runx1*-deficient mice at E17.5 compared to age-matched wild-type littermates. Concomitantly, vesicular acetylcholine transporter-positive axon terminals and acetylcholine receptor clusters were less dense in the V and T tongue muscles of *Runx1*-deficient mice. These abnormalities in axonal projection were not caused by a reduction in the total number hypoglossal neurons, failed synaptogenesis, or tongue muscles deficits. Our results implicate Runx1 in the targeting of ventrocaudal hypoglossal axons to specific tongue muscles. However, Runx1 deficiency did not alter neuronal survival or the expression of multiple motoneuron markers as in other neuronal populations. Thus, Runx1 appears to have distinct developmental functions in different brain regions.

INTRODUCTION

Runt-related (Runx) genes encode the DNA-binding α-subunit of the runt domain transcription factor farmily, also referred to as the polyomavirus enhancer-binding protein 2 (PEBP2)/core-binding factor (CBF) group. In *Drosophila*, the *runt* gene regulates multiple developmental processes, including segmentation and neuronal differentiation (Duffy et al., 1991; Dormand and Brand, 1998). In mammals, three Runx family transcription factors are crucial for the development of both neural and non-neural cells (for reviews, Ito, 2008; Stifani and Ma, 2009; Zagami et al., 2009).

Runx1 regulates the differentiation of hematopoietic cells in fetal liver, and its mutation is closely associated with human acute myeloid leukemia (De Brujin and Speck, 2004; Ito, 2004; Ichikawa et al., 2013). Runx1 is also expressed in the central and peripheral nervous systems (CNS and PNS). In the dorsal root ganglion (DRG), Runx1 is expressed initially in TrkA-positive small DRG neurons at early developmental stages (Levanon et al., 2001; Marmigère et al., 2006) and is involved in the cell type specification of non-peptidergic and peptidergic nociceptive neurons by repressing the expression levels of TrkA and calcitonin gene-related peptide (CGRP) and by promoting c-ret expression (Chen et al., 2006, Yoshikawa et al., 2007). Runx1 also regulates the expression of various ionic channels and receptors involved in sensing pain, itch, and/or temperature (Chen et al., 2006; Yoshikawa et al., 2007; Abdel Samad et al., 2010; Liu and Ma, 2011; Lopes et al., 2012; Yang et al., 2013). Recent studies reported that Runx1 is expressed in putative mechanoreceptors (Lou et al., 2013; Yoshikawa et al., 2013) and is required for the development of unmyelinated low-threshold mechanoreceptors (Lou et al., 2013). In addition to cell type specification, Runx1 is involved in the regulation DRG axon projections toward central and peripheral targets (Chen et al., 2006; Yoshikawa et al., 2007; Yang et al., 2013).

In the developing CNS, Runx1 is expressed by neuron subpopulations in the branchiovisceral motor nuclei of the hindbrain and spinal motor nuclei of the cervical cord (Theriault et al., 2004; Dansen et al., 2005; Stifani et al., 2008; Lamballe et al., 2011). Loss of Runx1 activity in the branchiovisceral nuclei induces cell death, suggesting that Runx1 is involved in the survival or proper maturation of branchiovisceral motoneurons (Theriault et al., 2004). In the spinal cord, both loss-of-function and gain-of-function studies suggest that Runx1 suppresses interneuron-specific developmental programs and maintains motoneuron characteristics

(Stifani et al., 2008). However, functional analysis of Runx1 in CNS development has been limited, and no studies have examined Runx1 function in axon targeting, in part because Runx1 deficiency results in lethality around embryonic day (E) 11.5 due to impaired fetal liver hematopoiesis (Okuda et al, 1996; Wang et al., 1996; Theriault et al., 2004, 2005). To overcome this limitation, we utilized transgenic *Runx1*$^{-/-}$ mice in which liver hematopoietic cells are selectively rescued by the expression of Runx1 under the control of the *GATA-1* promoter (Yokomizo et al., 2007). Selective rescue of Runx1 in hematopoietic cells enables these mice to survive until late embryonic stages.

Motoneurons of the hypoglossal nucleus (nXII) innervate tongue muscles. The topographic innervation of the tongue muscles by various nXII subpopulations has been revealed retrograde tracing (Aldes, 1995; Dobbins and Feldman, 1995; McClung and Goldberg, 1999, 2002). The nXII is divided into two major divisions, dorsal and ventral. Dorsal neurons project axons that form the lateral branch of the hypoglossal nerve (CN XII), whereas ventral neuron axons form the medial branch (Supporting Information Fig. S1; Dobbins and Feldman, 1995; Fregosi, 2011; Skouras et al., 2011). The lateral branch projects to the retractor muscles [extrinsic hypoglossus and styloglossus muscles, and intrinsic inferior and superior longitudinal (SL) muscles], whereas medial branch projects to the protruder muscles [extrinsic genioglossus (GG) muscle, and intrinsic vertical (V) and transverse (T) muscles] (Supporting Information Fig. S1; Fregosi, 2011). Within these circuits there is more precise myotopy; for example, most neurons of the ventrocaudal subdivision of rat nXII project to the intrinsic V and T muscles in the anterior tongue (Supporting Information Fig. S1; Aldes, 1995). However, the mechanisms that specify this precise neuron–muscle connectivity remain unclear (Fregosi, 2011).

In the present study, we examined the embryonic expression patterns of Runx1 in hypoglossal neurons and the roles of Runx1 in axon guidance and neuromuscular junction (NMJ) formation in the tongue of wild-type and *Runx1*-deficient mice.

MATERIALS AND METHODS

Animals

We examined the wild-type expression pattern of Runx1 in mouse embryos (C57BL/6J, Japan SLC, Inc., Japan). Runx1 function was examined in transgenic *Runx1*-deficient mice (*Runx1*$^{-/-}$*::Tg*) in which *GATA-1*-expressing hematopoietic cells are rescued by the *G1-HRD*-regulated expression of *Runx1*, whereas Runx1 expression remains deleted in most other cells, such as sensory and motor neurons (Yokomizo et al., 2007; Yoshikawa et al., 2007). These mice survive until late embryonic stages: and thus, we were able to analyze the roles of Runx1 in the development and targeting of hypoglossal axons. The *Runx1*$^{+/+}$*::Tg* littermates were used as controls. All experiments were approved by the Animal Care Committee of the University of Tsukuba or Nihon University School of Medicine.

Immunohistochemistry of the hypoglossal nucleus and tongues

Mouse embryos were perfused transcardially with 4% paraformaldehyde (PFA) in 0.1 M phosphate buffer (PB, pH 7.4) and immersed overnight (O/N) in the same fixative at 4°C. The heads were removed, immersed successively in 10%, 20%, and 30% sucrose in 0.1 M PB and frozen in Tissue Tek OCT compound (Sakura Finetek Japan). Frontal and sagittal sections were cut at 12–16-μm thickness using a cryostat (HM 500 OM, MICROM International GmbH) and collected on MAS-coated glass slides (Matsunami Glass). If needed, sections were subjected to epitope retrieval by heating to 105°C for 5 min in REAL Target Retrieval Solution (Dako). After treatment for 30 min at room temperature (RT) with 0.3% H_2O_2 in methanol, the sections were incubated for 1 h at RT in a blocking solution containing 5% normal serum and 0.1%–0.3% TritonX-100 in phosphate-buffered saline. The following primary antibodies were used in single-staining studies with peroxidase visualization: rabbit anti-Runx1 (Sigma-Aldrich; 1:1000 dilution), mouse anti-Runx1 (a gift from Dr. Y. Ito; 1:1000), rabbit anti-CGRP (Chemicon; 1:4000), rabbit anti-choline acetyltransferase (ChAT) (Millipore; 1:600), and mouse anti-myosin (MF 20; Developmental Studies Hybridoma Bank; 1:400). The sections were incubated O/N to 2 O/N at 4°C with one of the primary antibodies in the blocking solution, and then with a biotinylated secondary antibody (Vector Laboratories; 1:500) for 1 h at RT. Immunolabeled sections were then incubated with the peroxidase-conjugated avidin-biotin complex (Vector Laboratories, 1:100) for 30

min at RT and the positive reactions visualized with 3,3'-diaminobenzidine (DAB) using the ImmunoPure Metal-Enhanced DAB Substrate Kit (Pierce). The sections were observed using a light microscope (AxioPlan 2, Carl Zeiss). For double-immunostaining, the sections were incubated O/N to 2 O/N at 4°C with (1) mouse anti-Runx1 (a gift from Dr. Y. Ito; 1:500) plus either rabbit anti-ChAT (Millipore; 1:600) or rabbit anti-CGRP (Chemicon; 1:2000), (2) rabbit anti-Runx1 (Sigma-Aldrich; 1:500) plus goat anti-c-Met (R&D systems; 1:200), or (3) mouse anti-Islet-1/2 (39.4D5; Developmental Studies Hybridoma Bank; 1:200) plus either rabbit anti-CGRP (1:2000), goat anti-c-Met (1:200), rabbit anti-c-ret (Immuno-Biological Laboratories; 1:50), or goat anti-Frizzled3 (R&D Systems; 1:50). The sections were then incubated with Alexa Fluor 488-labeled and 594-labeled secondary antibodies (Invitrogen, 1:500) for 1 h at RT. Immunostained sections were observed at ×20 with a confocal laser scanning microscope (LSM510META ver3.2, Carl Zeiss) or a fluorescence microscope (BIOREVO BZ-9000, Keyence). Both *Runx1*$^{-/-}$*::Tg* and *Runx1*$^{+/+}$*::Tg* littermates were processed simultaneously.

Cell counting

For the analysis of Islet-1/2-positive/CGRP-negative cell number, serial frontal sections were cut throughout the nXII and every fifth section (12 μm) was stained with rabbit anti-CGRP (Chemicon; 1:2000) and mouse anti-Islet-1/2 (39.4D5; Developmental Studies Hybridoma Bank; 1:200) O/N at 4°C. Alexa Fluor 488-labeled and 594-labeled secondary antibodies were used for detection. Islet-1/2-positive/CGRP-negative cell number in each section was counted and the total number of these neurons was calculated.

Tracing axonal projections

Sagittal sections (12 μm) or frontal sections (16 μm) were incubated with rabbit anti-neurofilament 200 (NF-H, Sigma-Aldrich; 1:500) O/N at 4°C. An Alexa Fluor 488-labeled secondary antibody was used for detection. Acetylcholine receptor (AChR) clusters (axonal projection sites) localized at postsynaptic sites were identified using Alexa Fluor 594-labeled α-bungarotoxin (α-BTX, Invitrogen; 1:500).

Measurement of axon terminal area

Serial sagittal sections (12 μm) were cut using a cryostat and every fifth section was stained with primary antibodies against vesicular acetylcholine transporter (VAChT, Chemicon; 1:500) and CGRP (Chemicon, 1:2000) O/N at 4°C. Alexa Fluor 488-labeled and 594-labeled secondary antibodies were used for detection. Photomicrographs of three sections per mouse were acquired and analyzed. We divided sagittal images spanning from the tip to the base of the tongue into three areas: anterior body, posterior body, and base of the tongue (Supporting Information Fig. S2). For each section, six 200 × 200 μm or 200 × 600 μm regions were analyzed. In addition, a 100 × 100 μm unstained region was analyzed for subtraction of background.

Quantification of functional NMJ number

For analysis of presynaptic NMJ bouton density (Maeda et al., 2004; Vinsant et al., 2013), every second frontal section (16 μm) was stained with anti-VAChT and an Alexa Fluor 488 secondary antibody. AChR clusters localized in postsynaptic sites were identified with Alexa Fluor 594-labeled α-BTX (Invitrogen; 1:500). Any NMJ that had no sign of VAChT immunoreactivity was counted as denervated. For each area, 10–20 sections were counted and results are presented as % area of anti-VAChT staining per section and number of AChR clusters per section.

Retrograde labeling of motoneurons

A pregnant mouse at 17 days postcoitum was anesthetized using isoflurane and the uterus was pulled out of the abdominal cavity. An incision was made to expose the mouths of the embryos. Alexa Fluor 594-labeled cholera toxin B subunit (CTB, Invitrogen) was injected locally (1 μg/μl in saline; 0.5 μl volume) into the GG muscle of the embryonic tongue using an ultra-thin stainless-steel needle (2-SV100A5-5, Altair Corporation; 100 μm OD) connected to a microinjector (IM-300, Narishige). Following injection, surgical incisions in the uterine wall were closed. The uterus was then repositioned in the abdominal cavity, and the abdominal wall and skin were closed to allow the embryos to continue normal development. Embryos were removed and perfused transcardially with 4% PFA 3–24 h after injection. Serial cryostat sections (12 μm) were cut, and then incubated with rabbit anti-CGRP (Chemicon; 1:2000) O/N at 4°C followed by incubation with Alexa Fluor 488-labeled secondary antibody (Invitrogen; 1:500) for 1 h at RT. All CGRP-negative GG motoneurons (presumptive

Runx1-positive) in the hypoglossal nucleus were analyzed.

Quantification of fluorescence intensity

For quantification of the Fzd3 immunoreactivity in hypoglossal neurons, the signal intensity of Fzd3-positive motoneurons which expressed Islet-1/2 was measured using ImageJ (NIH). The signal intensity was expressed as average fluorescence intensity per cell. At least 280 neurons from each genotype were measured.

Measurement of tongue volume

Using every fifth frontal section (12 μm) containing whole tongues at E17.5, the areas of tongues in each section were measured and the tongue volume was calculated.

RESULTS

Co-localization of Runx1 with ChAT but not CGRP in the hypoglossal nucleus

In wild-type (WT) E17.5 mouse embryos, the strong Runx1 expression was detected in the ventrocaudal subdivision of nXII (ventrocaudal nXII) (Fig. 1A,B). To determine the functions of these neurons, sections of nXII were doubled stained for Runx1 and ChAT, which is expressed by hypoglossal motoneurons (Takami et al., 1985; Trifonov et al., 2009). Virtually, all cells in nXII expressed ChAT (Fig. 1C), including Runx1-positive cells (Fig. 1D,E), suggesting that Runx1-positive cells are cholinergic motoneurons. However, many ChAT-positive neurons did not express Runx1 (Fig. 1E). Therefore, there are two neuronal subpopulations in nXII, ChAT-positive/Runx1-positive, and ChAT-positive/Runx1-negative.

We also examined the co-localization of Runx1 with two other hypoglossal motoneuron markers, CGRP or c-Met (Takami et al., 1985; Terrado et al., 1999; Caton et al., 2000; Wu and Levitt, 2013). In contrast to ChAT expression, few Runx1-positive cells expressed CGRP or c-Met in nXII at E17.5 (Fig. 1F-K). Runx1-positive neurons were restricted to the ventral division of the caudal nXII, whereas CGRP-positive and c-Met-positive neurons were localized to the dorsal division. This reciprocal expression of Runx1 and CGRP was detected as early as E13.5 (Fig. 1L-N).

Conserved expression of motoneuron markers in *Runx1*$^{-/-}$*::Tg* hypoglossal nucleus

In *Runx1*-deficient mice engineered to express β-gal in all neurons normally expressing Runx1, the number of spinal motor neurons co-expresing β-gal and ChAT was reduced (Stifani et al., 2008), suggesting that Runx1 expression may be involved in the positive regulation of ChAT. However, in the E17.5 ventrocaudal nXII, similar numbers of ChAT-positive cells were observed in *Runx1*$^{+/+}$*::Tg* and *Runx1*$^{-/-}$*::Tg* mice (26.30 ± 0.84/section vs. 24.85 ± 1.13/section, mean of 20 sections from four embryos for each genotype; Fig. 2A,B). We also examined the expression of two markers of cranial motoneurons, Islet-1/2 (Varela-Echavarría et al., 1996; Caton et al., 2000) and c-ret (Yu et al., 1998; Mikaels et al., 2000; Tamura et al., 2003). The total number of Islet-1/2-positive/CGRP-negative cells was similar in *Runx1*$^{-/-}$*::Tg* and *Runx1*$^{+/+}$*::Tg* mice (588.75 ± 8.75 vs. 567.50 ± 12.5; $p = 0.21$, Fig. 2E,G,H,J). Runx1 regulates c-ret expression in DRG neurons (Chen et al., 2006; Yoshikawa et al., 2007). However, c-ret expression in nXII did not differ between *Runx1*$^{+/+}$*::Tg* and *Runx1*$^{-/-}$*::Tg* mice (Fig.

2K,L). Thus, three features of the motor neuron phenotype (ChAT, Islet-1/2, and c-ret expressions) are maintained in the nXII even in the absence of Runx1, strongly suggesting that Runx1 is not necessary for maintenance of motor neuron phenotype. This Runx1-independence of hypoglossal motoneuron phenotype differs from embryonic spinal motoneurons, which follow the interneuron lineage in the absence of Runx1 (Stifani et al., 2008). Furthermore, unlike DRG neurons, CGRP expression is maintained in the absence of Runx1. As shown above, CGRP was not expressed in Runx1-positive cells in the ventrocaudal nXII of WT mice (Fig. 1F-H). The reciprocal expression of Runx1 and CGRP suggests CGRP downregulation by Runx1, as in the case of DRG neurons (Chen et al., 2006; Yoshikawa et al., 2007). However, CGRP expression was not detected in the ventrocaudal nXII of *Runx1*$^{-/-}$*::Tg* mice (Fig. 2C,D,F,I), indicating that Runx1 alone can not suppress CGRP expression in nXII. A recent study reported that c-Met is required for CGRP expression in DRG together with Runx1 repression (Gascon et al., 2010). Expression of c-Met in nXII (Caton et al., 2000; Wu and Levitt, 2013) was similar in the nXII of *Runx1*$^{+/+}$*::Tg* and *Runx1*$^{-/-}$*::Tg* mice (Fig. 2M,N).

Altered hypoglossal axonal projections in *Runx1*$^{-/-}$*::Tg* tongue muscles

Runx1 is expressed in neurons of the ventrocaudal nXII (Fig. 1A,B), neurons that innervate the intrinsic V and T muscles and extrinsic GG muscle through the medial branch of CN XII (Supporting Information Fig. S1; Aldes, 1995), suggesting that Runx1 may be involved in axonal pathfinding to these muscles. Thus, we examined axonal projections to the intrinsic V and T muscles in *Runx1*$^{-/-}$*::Tg* and *Runx1*$^{+/+}$*::Tg* mice. We prepared both sagittal and frontal sections of the tongue at E17.5 and stained them with NF-H antibody. In *Runx1*$^{+/+}$*::Tg* mice, hypoglossal axons ran longitudinally in the superficial region of the tongue and projected collaterals to the core region, forming a comb-like structure (Fig. 3A; Mbiene and Mistretta, 1997). In contrast to these normal longitudinal axon bundles, hypoglossal axons were sparse in the core region of the tongue of *Runx1*$^{-/-}$*::Tg* mice (Fig. 3D). In addition, some hypoglossal axons were truncated and less tightly bundled in the V and T tongue muscles of *Runx1*$^{-/-}$*::Tg* mice (Fig. 3J,O,P; Sokoloff and Burkholder, 2013). These results suggest that Runx1 in ventrocaudal hypoglossal neurons mediates axonal pathfinding to the V and T tongue muscles.

Reduced number of hypoglossal axon terminals in the V and T tongue muscles of *Runx1*$^{-/-}$*::Tg* mice

Aldes (1995) reported that motoneurons in the ventrocaudal nXII project to the intrinsic V and T muscles in the anterior part of the tongue (Supporting Information Fig. S1). To examine if ventrocaudal projections to the V and T muscles from (normally) Runx1-positive neurons are altered by the absence of Runx1, we compared the total axon terminal areas in the V and T muscles of *Runx1*$^{-/-}$*::Tg* and *Runx1*$^{+/+}$*::Tg* mice. We divided the tongue into three anteroposterior regions, the anterior body, posterior body, and the base, and identified axon terminals in the V and T muscles by VAChT expression (Supporting Information Fig. S2 for detailed procedure). Expression of CGRP and Runx1 were mutually exclusive and CGRP expression was not changed in the nXII of *Runx1*$^{-/-}$*::Tg* mice (Fig. 1); CGRP-positive and CGRP-negative axon terminals were assumed to arise from Runx1-negative and Runx1-positive neurons, respectively.

Sagittal sections were double-labeled with antibodies for VAChT, a general marker for motor axon terminals (Kobayashi et al., 2011), and CGRP, which has also been localized to motor axon terminals (Sato et al., 2011). Then, we analyzed three types of axon terminals, VAChT-positive, CGRP-positive, and VAChT-positive/CGRP-negative, representing all hypoglossal neurons, presumptive Runx1-negative hypoglossal neurons, and presumptive Runx1-positive hypoglossal neurons, respectively. In *Runx1*$^{+/+}$*::Tg* mice, the area of VAChT-positive axon terminals was similar among the three tongue regions (Fig. 4A,G), indicating a relatively equal distribution. The area of CGRP-positive axon terminals (from Runx1-negative neurons) was smaller in the anterior body than in other regions (Fig. 4B,H), whereas the area of VAChT-positive/CGRP-negative axon terminals (from Runx1-positive neurons) was larger in the anterior body (Fig. 4C,I), consistent with the reported topographic innervation patterns of hypoglossal neurons (Fig. 4H-J; Aldes, 1995). In *Runx1*$^{-/-}$*::Tg* mice, the area of VAChT-positive axon terminals was reduced to 64% of control (*Runx1*$^{+/+}$*::Tg* mice) in the anterior body, to 50% in the posterior body, and to 46% in the base ($p < 0.05$) (Fig. 4A,D,G), indicating an overall reduction in innervation density. The area of CGRP-positive (presumptive normally Runx1-negative) axon terminals was were not altered relative to *Runx1*$^{+/+}$*::Tg* mice (Fig. 4B,E,H), but the area of

VAChT-positive/CGRP-negative axon terminals (arising from neurons normally expressing Runx1) was significantly reduced in all three regions (to 30%, 36%, and 32% of *Runx1*$^{+/+}$*::Tg* mice, respectively; $p < 0.05$) (Fig. 4C,F,I). Thus, Runx1 deficiency decreased innervation from the nXII to the V and T tongue muscles, consistent with a role in axon pathfinding to target muscles.

Reduced NMJ numbers in the V and T tongue muscles in *Runx1*$^{-/-}$*::Tg* mice

We then assessed whether Runx1 deficiency influenced the formation of NMJs in the V and T tongue muscles by analyzing VAChT-positive axon terminals and α-BTX-positive (α-BTX^{+}) AChR clusters localized at the postsynaptic sites (Sokoloff and Burkholder, 2013). The distribution of AChR clusters appeared normal in *Runx1*$^{-/-}$*::Tg* mice (Figs 5B,E, 9C,D,F,G). However, the number of α-BTX^{+} AChR clusters was significantly reduced in the anterior body, posterior body, and base of *Runx1*$^{-/-}$*::Tg* V and T tongue muscles compared to *Runx1*$^{+/+}$*::Tg* mice (Fig. 5G). Specifically, the number of α-BTX^{+} AChR clusters was reduced in the anterior body, posterior body, and base of the V muscle (Fig. 5H) and in the anterior and posterior body of the T muscle (Fig. 5I). However, most NMJs were still innervated in *Runx1*$^{-/-}$*::Tg* mice and % innervation was not significantly different from *Runx1*$^{+/+}$*::Tg* (Fig. 5J), suggesting that Runx1 is not involved in NMJ formation once the target muscle is reached.

We also examined whether aberrant axonal projection leads to failure to form proper NMJs, or to maintain them by analyzing E13.5 and E15.5 embryos. At E13.5, entry of hypoglossal axons into the body of the tongue was observed (Supporting Information Fig. S3A) but NMJs were immature (data not shown; Yamane et al., 2001). At E13.5, the hypoglossal axons were sparse in *Runx1*$^{-/-}$*::Tg* tongue (Supporting Information Fig. S3B). Thereafter at E15.5, NMJs without innervation were observed in *Runx1*$^{-/-}$*::Tg* tongue (Supporting Information Fig. S3C-H). Thus, reduction of axon terminals and AChR clusters in the V and T muscles in *Runx1*$^{-/-}$*::Tg* mice at E17.5 seem to be due to the deficiency of axonal growth into the muscles.

Increased axon terminal area in *Runx1*$^{-/-}$*::Tg* GG tongue muscle

We examined whether axonal projections to the extrinsic GG muscle and intrinsic SL muscle, innervated by the medial and lateral branches of CN XII, respectively, are

altered by Runx1 deficiency. In contrast to V and T muscles (Fig. 4), the area of VAChT-positive axon terminals was higher in the extrinsic GG muscle of *Runx1*$^{-/-}$*::Tg* mice relative to *Runx1*$^{+/+}$*::Tg* mice (120%; $p < 0.05$) (Fig. 6A,D,G), whereas no changes were observed in the SL muscle (Fig. 6H), suggesting that Runx1 deficiency alters axon terminals primarily in muscles supplied by the medial branch. Similar to results in V and T muscles, most AChR clusters in the GG muscle were innervated in both *Runx1*$^{+/+}$*::Tg* and *Runx1*$^{-/-}$*::Tg* mice (Fig. 6I). The number of AChR clusters was not changed in *Runx1*$^{-/-}$*::Tg* GG muscle (Fig. 6J), and the distribution of AChR clusters appeared normal in *Runx1*$^{-/-}$*::Tg* mice (Fig. 6B,E). The number of AChR clusters was also similar in IL, HY, and STY muscles in *Runx1*$^{+/+}$*::Tg* and *Runx1*$^{-/-}$*::Tg* mice (IL, 8.63 ± 1.16/section vs. 7.78 ± 0.78/section; HY, 5.85 ± 1.31/section vs. 4.45 ± 0.99/section; STY, 7.78 ± 0.64/section vs. 6.58 ± 1.09/section).

Hypoglossal axonal projections to the extrinsic GG muscles in *Runx1*$^{-/-}$*::Tg* mice

Reduced VAChT area in the intrinsic V and T muscles (Fig. 4) and concomitant greater area in the extrinsic GG muscle in *Runx1*$^{-/-}$*::Tg* mice (Fig. 6) suggest that some hypoglossal neurons switch targets in the absence of Runx1. To address this possibility, we examined hypoglossal neurons using retrograde labeling. CTB was injected into the GG muscle of E17.5 embryos, and the localization of CTB-labeled motoneurons was examined 3–4 h later. To focus on Runx1-expessing neurons, the tissues were stained with CGRP and all CGRP-negative neurons were identified as Runx1-positive neurons. In *Runx1*$^{+/+}$*::Tg* mice, CTB-labeled hypoglossal neurons coexpressed CGRP and were localized to the lateral region of the ventrocaudal nXII, suggesting that the GG muscle is innervated by Runx1-negative motoneurons (Figs 7A-C, Supporting Information S1A,C). Axon terminal area was increased in *Runx1*$^{-/-}$*::Tg* GG muscle; thus, some hypoglossal neurons may project ectopic axons to the GG muscle in the absence of Runx1. However, CTB-labeling was still restricted to CGRP-positive hypoglossal neurons in *Runx1*$^{-/-}$*::Tg* mice (Fig. 7D-F), suggesting that the ventrocaudal hypoglossal neurons which are supposed to express Runx1 do not project to the GG muscle in substantial numbers in the absence of Runx1.

The expression of Fzd3 in *Runx1*$^{-/-}$*::Tg* hypoglossal nucleus

A recent study reported that the Wnt receptor Frizzled3 (Fzd3) also contributes to

axonal pathfinding of hypoglossal neurons (Hua et al., 2013; Hua et al., 2014) as tongue muscle innervation was reduced in *Fzd3*-deficient mice. Considering the similar phenotypes of *Fzd3*-deficient and *Runx1*-deficient mice, it is possible that Fzd3 may mediate the effects of Runx1. Fzd3 expression was reduced in the nXII of *Runx1*$^{-/-}$*::Tg* mice (877.1 ± 48.4, $p < 0.005$) (Fig. 8D,F,G) compared to *Runx1*$^{+/+}$*::Tg* mice (1956.5 ± 199.0) (Fig. 8A,C,G), suggesting that Runx1 promotes Fzd3 expression. Further studies are necessary to determine whether Runx1 mediates axonal pathfinding of hypoglossal neurons through Fzd3.

Runx1 deficiency has no effects on tongue muscles

An alternative explanation for these results is that altered axonal projections to the tongue are caused by abnormalities in the tongue muscle as muscles provide cues for both axon guidance and synaptogenesis. To examine this possibility, we first examined the expression of Runx1 in WT tongue at E17.5. Runx1 was detected in connective tissue papilla but not in tongue muscles (Fig. 9A). In sections stained with hematoxylin and eosin, the overall size of the tongue (*Runx1*$^{+/+}$*::Tg* mice, 5.92 ± 0.30 mm^3 vs. *Runx1*$^{-/-}$*::Tg* mice, 6.07 ± 0.19 mm^3) and the morphology of the tongue muscles were not noticeably altered in *Runx1*$^{-/-}$*::Tg* mice, although there were minor differences in the interstitial tissue space around the tongue tip. There was also no significant difference in myosin expression in *Runx1*$^{-/-}$*::Tg* tongue muscles (Fig. 9B,E). In addition, the number of myofibrils in V and T muscles was similar in *Runx1*$^{+/+}$*::Tg* and *Runx1*$^{-/-}$*::Tg* mice (for V muscle, 31.2 ± 1.76/section vs. 29.7 ± 2.75/section; for T muscle, 32.2 ± 1.02/section vs. 31.0 ± 1.55/section). These results suggest that the abnormalities in axonal projections are mainly attributable to deficient of Runx1 in hypoglossal neurons rather than Runx1-dependent changes in muscle signaling and function.

DISSCUTION

In the present study, we mapped Runx1 expression in hypoglossal neurons of mouse embryos and examined the roles of Runx1 in cell type specification and axonal pathfinding to tongue muscles. In nXII, Runx1-positive neurons were located in the ventrocaudal subdivision. These Runx1-positive neurons did not express CGRP, and

CGRP-positive neurons did not express Runx1. Expression of CGRP was not changed in *Runx1*-deficient mice, indicating that Runx1-mediated CGRP downregulation is not responsible for this mutually exclusive expression pattern. Runx1 deficiency altered axonal projections to selected tongue muscles and concomitantly reduced the density of axon terminals and postsynaptic AChR clusters. In contrast, Runx1 deficiency did not alter the number of hypoglossal neurons or the proportion of synapses containing both presynaptic and postsynaptic elements (VAChT and AChR clusters, respectively). Taken together, these results suggest that Runx1 is involved in targeting ventrocaudal hypoglossal neurons to specific muscles but is not necessary for neuronal survival, motoneuron specification, or synaptic development.

Expression of Runx1 in hypoglossal nucleus

Previous studies using *Runx1 lacZ*/+ mice in which *β-gal* gene was inserted into the *Runx1* locus to produce a Runx1–β-gal fusion protein implicated Runx1 expression in the regional control of brain development (Levanon et al., 2001; Theriault et al., 2004). In contrast to DRG, spinal motoneurons, and other brainstem population, the pattern of Runx1 expression in hypoglossal neurons and the function of Runx1 in survival, differentiation, and axonal pathfinding in nXII had not been studied.

Immunohistochemical staining of WT mice revealed that Runx1 expression in nXII is limited to the ventrocaudal subdivision at E17.5, a subdivision previously shown to project to both the intrinsic V and T muscles and the extrinsic GG muscle in the tongue (Aldes, 1995). Runx1 deficiency markedly reduced axonal projections to the V and T tongue muscles, while producing a very modest increase in GG innervation strongly suggesting that pathfinding (but not survival or synaptogenesis) is dependent on Runx1 expression.

Regulation of ChAT, Islet-1/2, and CGRP expressions

In the spinal cord of mouse embryos, Runx1 is expressed in selected motoneuron subtypes in the cervical spinal cord (Dansen et al., 2005; Stifani et al., 2008; Lamballe et al., 2011). In the spinal cord of *Runx1*-deficient mice (E13.5 and 18.5), there were fewer neurons expressing motoneuron-specific markers such as ChAT and Islet-1/2, and more neurons expressing interneuron-specific markers such as Pax2 (Stifani et al., 2008), implicating Runx1 in lineage specification of spinal motoneurons. Moreover,

overexpression of *Runx1* in the chick spinal cord decreased the expression of interneuron-specific markers and increasing expression of motoneuron-specific markers. These results suggest that Runx1 suppresses interneuron-specific developmental programs and maintains motoneuron characteristics in the spinal cord (Stifani et al., 2008). Similar functions of Runx1 and Runx3 in neuronal subtype specification from bipotential or multipotential neuronal progenitors have been demonstrated during development of PNS sensory neurons (for reviews, Inoue et al., 2008; Lallemend and Ernfors, 2012). Conversely, in the nXII, a region predominantly populated by motoneurons with few interneurons (Takasu and Hashimoto, 1988; Sturrock, 1991), ChAT and Islet-1/2 expression levels were not altered by Runx1 deficiency. Thus, Runx1 does not contribute substantially to survival or maintenance of the motoneuron phenotype in the nXII.

CGRP is also expressed in the nXII (Takami et al., 1985; Terrado et al., 1999), and our immunohistochemical results showed that the nXII contains two distinct and non-overlapping motoneuron populations, Runx1-negative/CGRP-positive and ventrocaudal Runx1-positive/CGRP-negative. Previous studies reported that CGRP expression is upregulated in the DRG of *Runx1*-deficient mice, suggesting that Runx1 suppresses CGRP expression (Chen et al., 2006; Kramer et al., 2006; Yoshikawa et al., 2007). The reciprocal expression of Runx1 and CGRP in nXII also suggests that CGRP is suppressed by Runx1. However, CGRP expression was still lost in the ventrocaudal nXII of *Runx1*-decicient mice and maintained elsewhere in the nXII, indicating that Runx1 is not sufficient to suppress CGRP expression in the nXII. Alternatively, hepatocyte growth factor (HGF)–c-Met signaling both represses Runx1 expression and induces CGRP expression in DRG neurons (Gascon et al., 2010). In addition, Runx1 and c-Met are reciprocally regulated in DRG neurons (Gascon et al., 2010). However, c-Met expression was still absent in the ventrocaudal nXII of *Runx1*-decicient mice. In contrast to DRG, Runx1 is positively regulated by c-Met in spinal motor neurons (Lamballe et al., 2011). The relationships among Runx1, c-Met, and CGRP in the hypoglossal neurons appear distinct from those described in spinal motoneurons or DRG neurons.

Roles of Runx1 in myotopic axonal projection to the tongue

Axonal projection to specific targets during development is crucial for proper motor

function. Runx1 is expressed in selected sensory neurons where it regulates axonal projection to specific targets (Chen et al., 2006; Yoshikawa et al., 2007; Yang et al., 2013). The present study demonstrates a similar function in the nXII, with Runx1 expression necessary for axonal projection from the ventrocaudal nXII to intrinsic V and T muscles of the tongue. In contrast to the effects of Runx1 deficiency on projections to V and T muscles, there may have been a modest increase in presynaptic projections to the GG muscle, indicating that axons are not redirected to ectopic sites. Rather, immunohistochemical staining of serial sections revealed that Runx1-deficient axons were truncated and fasciculation was incomplete. Thus, Runx1 appears necessary for axonal organization in the CN XII as well as for axonal projection.

It is still unclear how axons of hypoglossal neurons are guided to spesific target muscles (Fregosi, 2011). Abnormal axonal projections of hypoglossal neurons were reported in mice deficient in HGF or its receptor (encoded by *c-Met*) (Caton et al., 2000), RhoA and Rho-kinase (Rho-K) (Kobayashi et al., 2011), and neuropilin-1 (Huettl and Huber, 2011). Knockout of neuropilin-1 from somatic motoneurons impaired the initial fasciculation and the assembly of hypoglossal rootlets but not later axon guidance (Huettl and Huber, 2011). In *Runx1*-deficient mice, nXII expression of c-Met was normal and initial projection and bundle formation of CN XII appeared normal at E11.5–E13.5 (data not shown). Thus, it is unlikely that the altered axonal projection from nXII in *Runx1*-deficient mice is associated with c-Met, HGF, RhoA, Rho-K, or neuropilin-1 dysfunction.

In $Ret^{Nkx6.2\text{-}Cre}$, *RhoA*, *Rho-K*, and *N-catenin* mutant mice, each with specifically deleted cranial motoneurons, axonal projections to the tongue muscles were reduced, together with a reduction in the number of hypoglossal neurons (Baudet et al., 2008; Kobayashi et al., 2011; Uemura and Takeichi, 2011). A reduction in axonal projection was also observed in *Runx1*-deficient mice, but there was no detectable reduction in the number of hypoglossal neurons. A recent study reported that Fzd3 controls axonal projection of hypoglossal neurons (Hua et al., 2013; Hua et al., 2014). The expression of Fzd3 was lower in the nXII of *Runx1*-deficient mice, suggesting a functional association of Runx1 with Fzd3 in axonal projection. In addition, Fzd3 deficiency also caused cell death of some cranial and spinal neurons (Hua et al., 2013), but reduced Fzd3 expression was not associated with reduced neuronal survival in the nXII. Thus, Runx1 appears specialized for axonal growth and or pathfinding in the nXII, possibly by

interacting with Fzd3, but unlike Ret, RhoA, Rho-K, or N-catenin, does not contribute to progenitor proliferation or neuronal survival.

Specific myotopic axon projections require the coordinated activity of multiple guidance and growth factors (Bonanomi and Pfaff, 2010; Demireva et al., 2011; Bonanomi et al., 2012; Hua et al., 2013; Hua et al., 2014). For example, both loss of *Nkx6.1* expression and ectopic *Nkx6.1* expression alter the position of selected motor pools in the spinal cord and redirect axons to new muscle targets (De Marco Garcia and Jessell, 2008). In *Runx1*-deficient mice, axon terminals were decreased in the V and T muscles and increased slightly in the GG muscle, but no ectopic hypoglossal neurons were detected projecting to the GG muscle, suggesting that Runx1 deficiency altered axonal projection but did not switch the selectivity from the proper target muscles. Runx1 may regulate downstream factors that control motor axonal projection. The interaction of membrane bound ephrins with ephrin receptors (Ephs) guides axonal pathfinding through both repulsive and attractive interactions (Egea and Klein 2007; Reber et al., 2007). Indeed, ephrin–Eph signaling controls the topographic projections of a variety of neurons (Kao et al., 2012; Dudanova and Klein, 2013). A recent report showed that c-ret mediates Ephrin-A reverse signaling in motoneurons (Bonanomi et al., 2012). In addition, lack of c-ret in hypoglossal neurons resulted in a developmental deficit of axon terminal maturation (Baudet et al., 2008). We and others reported that Runx1 regulates c-ret expression in DRG neurons (Chen et al., 2006; Yoshikawa et al., 2007). However, c-ret expression was not changed in the nXII of *Runx1*-deficient mice. Taken together, our data demonstrate that Runx1 is critical for regulating axonal projections of specific hypoglossal neurons, but this function is likely independent of c-ret. The downstream molecular signaling pathways activated by Runx1 remain to be identified.

Intramuscular nerve branching defects in skeletal muscles, including the latissimus dorsi (LD), cutaneous maximus, and diaphragm, were reported in *Pea3*-deficient, *erbB2*-deficient, and *damage-induced neuronal endopeptidase* (*DINE*)-deficient mice (Lin et al., 2000; Haase et al., 2002; Livet et al., 2002; Nagata et al., 2010). DINE is expressed in CNS neurons, including hypoglossal neurons, and the PNS neurons from early development (Nagata et al., 2006). DINE deficiency resulted in altered arborization of intramuscular nerves in the diaphragm and LD muscles, whereas motoneurons and initial axonal outgrowth were normal (Nagata et al., 2010). Schwann

cells also affect fasciculation and generation of motor axons (Lin et al., 2000). In *Runx1*-deficient mice, hypoglossal axons branched normally from the main intramuscular nerve, but some axons were less tightly bundled and truncated. Runx1 also promoted axonal branching in neurogenin-2-fated boundary cap neural crest stem cells (Marmigère et al., 2006). Thus, loss of Runx1 may regulate axon–Schwann cell interactions in the tongue muscles to maintain appropriate pathfinding to target muscles or interact with other regulators of axonal branching, such as DINE.

NMJ formation

Formation of NMJs requires the coordinated interaction of neuronal-, Schwann cell-, and muscle-derived factors. Indeed, dysfunction of specific synaptogenic molecules in motor axons, terminal Schwann cells, or skeletal muscles can cause failure of NMJ formation (Witzemann, 2006; Wu et al., 2010; Ferraro et al., 2012; Hubbard and Gnanasambandan, 2013). For example, agrin, a heparin-sulfate proteoglycan secreted by motoneurons, induces clustering of AChRs on the postsynaptic side of the junction (muscle membrane). During diaphragm development, AChR clusters that first form in the middle region of diaphragm muscle fibers are enlarged if innervated but disappear if not (Wu et al., 2010). In *Runx1*-deficient mice, both axon terminals (VAChT-positive areas) and AChR clusters were reduced in V and T tongue muscles. However, most NMJs that remained were normally innervated, suggesting that Runx1 is not directly involved in NMJ formation.

Tongue muscles

The skeletal muscle proteins MuSK, LRP4, and rapsyn are critical for NMJ formation (Witzemann, 2006; Wu et al., 2010; Ferraro et al., 2012; Hubbard and Gnanasambandan, 2013). In *Runx1*-deficient mice, the distribution of AChR clusters appeared normal. In addition, Runx1 was expressed in connective tissue papilla of tongue but not in innervated skeletal muscles at E17.5. Moreover, Runx1 does not directly regulate AChR δ-subunit gene expression in developing muscles (Zhu et al., 1994). These results suggest that Runx1 does not affect skeletal muscles directly during late embryonic stages and likely functions via a presynaptic mechanism.

In conclusion, we demonstrate novel functions of Runx1 in axonal projection of

hypoglossal motor neurons. Runx1 deficiency perturbs the proper projection of hypoglossal axons to tongue muscles during embryonic development. Further studies are needed to identify the downstream targets of the Runx1 transcription factor. However, in contrast to other PNS and spinal neuron populations, Runx1 does not contribute to neuronal survival, maintenance of motoneuron phenotype, or synaptogenesis of hypoglossal neurons.

ACKNOWLEAGEMENTS

We thank Dr. Y. Ito (Cancer Science Institute of Singapore, National University of Singapore) for providing the antibody against Runx1. This study was supported by a Grant-in-Aid for Scientific Research (B) to T.S. from the Ministry of Education, Culture, Sports, Science and Technology (MEXT) of Japan.

REFERENCES

Abdel Samad O, Liu Y, Yang FC, Kramer I, Arber S, Ma Q. 2010. Characterization of two Runx1-dependent nociceptor differentiation programs necessary for inflammatory versus neuropathic pain. Mol Pain 6:45.

Aldes LD. 1995. Subcompartmental organization of the ventral (protrusor) compartment in the hypoglossal nucleus of the rat. J Comp Neurol 353:89–108.

Baudet C, Pozas E, Adameyko I, Andersson E, Ericson J, Ernfors P. 2008. Retrograde signaling onto Ret during motor nerve terminal maturation. J Neurosci 28:963–975.

Bonanomi D, Chivatakarn O, Bai G, Abdesselem H, Lettieri K, Marquardt T, Pierchala BA, Pfaff SL. 2012. Ret is a multifunctional coreceptor that integrates diffusible- and contact-axon guidance signals. Cell 148:568–582.

Bonanomi D, Pfaff SL. 2010. Motor axon pathfinding. Cold Spring Harb Perspect Biol 2:a001735.

Caton A, Hacker A, Naeem A, Livet J, Maina F, Bladt F, Klein R, Birchmeier C, Guthrie S. 2000. The branchial arches and HGF are growth-promoting and chemoattractant for cranial motor axons. Development 127:1751–1766.

Chen CL, Broom DC, Liu Y, de Nooij JC, Li Z, Cen C, Samad OA, Jessell TM, Woolf CJ, Ma Q. 2006. Runx1 determines nociceptive sensory neuron phenotype and is required for thermal and neuropathic pain. Neuron 49:365–377.

Dansen JS, Tice BC, Brennner-Morton S, Jessell TM. 2005. A hox regulatory network establishes motor neuron pool identity and target-muscle connectivity. Cell 123:477–491.

De Brujin MF, Speck NA. 2004. Core-binding factors in hematopoiesis and immune function. Oncogene 23:4238–4248.

De Marco Garcia NV, Jessell TM. 2008. Early motor neuron pool identity and muscle nerve trajectory defined by postmitotic restrictions in Nkx6.1 activity. Neuron 57:217–231.

Demireva EY, Shapiro LS, Jessell TM, Zampieri N. 2011. Motor neuron position and topographic order imposed by β- and γ-catenin activities. Cell 147:641–652.

Dobbins EG, Feldman JL. 1995. Differential innervation of protruder and retractor muscles of the tongue in rat. J Comp Neurol 357:376–394.

Dormand EL, Brand AH. 1998. Runt determines cell fates in the Drosophila embryonic CNS. Development 125:1659–1667.

Dudanova I, Klein R. 2013. Integration of guidance cues: parallel signaling and crosstalk. Trends Neurosci 36:295–304.

Duffy JB, Kania MA, Gergen JP. 1991. Expression and function of the Drosophila gene runt in early stages of neural development. Development 113:1223–1230.

Egea J, Klein R. 2007. Bidirectional Eph-ephrin signaling during axon guidance. Trends Cell Biol 17:230–238.

Ferraro E, Molinari F, Berghella L. 2012. Molecular control of neuromuscular junction development. J Cachexia Sarcopenia Muscle 3:13–23.

Fregosi RF. 2011. Respiratory related control of hypoglossal motoneurons--Knowing what we do not know. Respir Physiol Neurobiol 179:43–47.

Gascon E, Gaillard S, Malapert P, Liu Y, Rodat-Despoix L, Samokhvalos IM, Delmas P, Helmbaher F, Maina F, Moqrich A. 2010. Hepatocyte growth fator-Met signaling is required for Runx1 extinction and peptidergic differentiation in primary nociceptive neurons. J Neurosci 30:12414–12423.

Haase G, Dessaud E, Garcès A, de Bovis B, Birling M, Filippi P, Schmalbruch H, Arber S, deLapeyrière O. 2002. GDNF acts through PEA3 to regulate cell body positioning and muscle innervation of specific motor neuron pools. Neuron 35:893–905.

Hua ZL, Smallwood PM, Nathans J. 2013. Frizzled3 controls axonal development in distinct populations of cranial and spinal motor neurons. Elife 2:e01482.

Hua ZL, Chang H, Wang Y, Smallwood PM, Nathans J. 2014. Partial interchangeability of Fz3 and Fz6 in tissue polarity signaling for epithelial orientation and axon growth and guidance. Development 141:3944–3954.

Hubbard SR, Gnanasambandan K. 2013. Structure and activation of MuSK, a receptor tyrosine kinase central to neuromuscular junction formation. Biochim Biophys Acta 1834:2166–2169.

Huettl RE, Huber AB. 2011. Cranial nerve fasciculation and Schwann cell migration are impaired after loss of Npn-1. Dev Biol 359:230–241.

Ichikawa M, Yoshimi A, Nakagawa M, Nishimoto N, Watanabe-Okochi N, Kurokawa M. 2013. A role for RUNX1 in hematopoiesis and myeloid leukemia. Int J Hematol 97:726–734.

Inoue K, Shiga T, Ito Y. 2008. Runx transcription factors in neuronal development. Neural Dev 3:20.

Ito Y. 2004. Oncogenic potential of the RUNX gene family: overview. Oncogene 23:4198–4208.

Ito Y. 2008. RUNX genes in development and cancer: regulation of viral gene expression and the discovery of RUNX family genes. Adv Cancer Res 99:33–76.

Kao TJ, Law C, Kania A. 2012. Eph and ephrin signaling: lessons learned from spinal motor neurons. Semin Cell Dev Biol 23:83–91.

Kobayashi K, Masuda T, Takahashi M, Miyazaki J, Nakagawa M, Uchigashima M, Watanabe M, Yaginuma H, Osumi N, Kaibuchi K, Kobayashi K. 2011. Rho/Rho-kinase signaling pathway controls axon patterning of a specified subset of cranial motor neurons. Eur J Neurosci 33:612–621.

Kramer I, Sigrist M, de Nooji JC, Taniuchi I, Jessell TM, Arber S. 2006. A role for Runx transcription factor signaling in dorsal root ganglion sensory neuron diversification. Neuron 49:379–393.

Lallemend F, Ernfors P. 2012. Molecular interactions underlying the specification of sensory neurons. Trends Neurosci 35:373–381.

Lamballe F, Genestine M, Caruso N, Arce V, Richelme S, Helmbacher F, Maina F. 2011. Pool-specific regulation of motor neuron survival by neurotrophic support. J Neurosci 31:11144–11158.

Levanon D, Brenner O, Negreanu V, Bettoun D, Woolf E, Eilam R, Lotem J, Gat U, Otto F, Speck N, Groner Y. 2001. Spatial and temporal expression pattern of Runx3 (Aml2) and Runx1 (Aml1) indicates non-redundant functions during mouse embryogenesis. Mech Dev 109:413–417.

Lin W, Sanchez HB, Deerinck T, Morris JK, Ellisman M, Lee KF. 2000. Aberrant development of motor axons and neuromuscular synapses in erbB2-deficient mice. Proc Natl Acad Sci USA 97:1299–1304.

Liu Y, Ma Q. 2011. Generation of somatic sensory neuron diversity and implications on sensory coding. Curr Opin Neurobiol 21:52–60.

Livet J, Sigrist M, Stroebel S, De Paola V, Price SR, Henderson CE, Jessell TM, Arber S. 2002. ETS gene Pea3 controls the central position and terminal arborization of specific motor neuron pools. Neuron 35:877–892.

Lopes C, Liu Z, Xu Y, Ma Q. 2012. Tlx3 and Runx1 act in combination to coordinate the development of a cohort of nociceptors, thermoceptors, and pruriceptors. J Neurosci 32:9706–9715.

Lou S, Duan B, Vong L, Lowell BB, Ma Q. 2013. Runx1 controls terminal morphology and mechanosensitivity of VGLUT3-expressing C-mechanoreceptors. J Neurosci 33:870–882.

Maeda M, Ohba N, Nakagomi S, Suzuki Y, Kiryu-Seo S, Namikawa K, Kondoh W, Tanaka A, Kiyama H. 2004. Vesicular acetylcholine transporter can be a morphological marker for the reinnervation to muscle of regenerating motor axons. Neurosci Res 48:305–314.

Marmigère F, Montelius A, Wegner M, Groner Y, Reichardt LF, Ernfors P. 2006. The Runx1/AML1 transcription factor selectively regulates development and survival of TrkA nociceptive sensory neurons. Nat Neurosci 9:180–187.

Mbiene JP, Mistretta CM. 1997. Initial innervation of embryonic rat tongue and developing taste papillae: nerves follow distinctive and spatially restricted pathways. Acta Anat 160:139–158.

McClung JR, Goldberg SJ. 1999. Organization of motoneurons in the dorsal hypoglossal nucleus that innervate the retrusor muscles of the tongue in the rat. Anat Rec 254:222–230.

McClung JR, Goldberg SJ. 2002. Organization of the hypoglossal motoneurons that innervate the horizontal and oblique components of the genioglossus muscle in the rat. Brain Res 950:321–324.

Mikaels A, Livet J, Westphal H, De Lapeyrière O, Ernfors P. 2000. A dynamic regulation of GDNF-family receptors correlates with a specific trophic dependency of cranial motor neuron subpopulations during development. Eur J Neurosci 12:446–456.

Nagata K, Kiryu-Seo S, Kiyama H. 2006. Localization and ontogeny of damage-induced neuronal endopeptidase mRNA-expressing neurons in the rat nervous system. Neuroscience 141:299–310.

Nagata K, Kiryu-Seo S, Maeda M, Yoshida K, Morita T, Kiyama H. 2010. Damage-induced neuronal endopeptidase is critical for presynaptic formation of neuromuscular junctions. J Neurosci 30:6954–6962.

Okuda T, van Deursen J, Hiebert SW, Grosveld G, Downing JR. 1996. AML1, the target of multiple chromosomal translocations in human leukemia, is essential for normal fetal liver hematopoiesis. Cell 84:321–330.

Reber M, Hindges R, Lemke G. 2007. Eph receptors and ephrin ligands in axon guidance. Adv Exp Med Biol 621:32–49.

Sato T, Shimizu Y, Kano M, Suzuki T, Kanetaka H, Chu LW, Côté PD, Shimauchi H, Ichikawa H. 2011. Increase of CGRP expression in motor endplates within fore and hind limb muscles of the degenerating muscle mouse (Scn8a(dmu)). Cell Mol Neurobiol 31:155–161.

Skouras E, Ozsoy U, Sarikcioglu L, Angelov DN. 2011. Intrinsic and therapeutic factors determining the recovery of motor function after peripheral nerve transection. Ann Anat 193:286–303.

Sokoloff A, Burkholder T. 2013. Tongue Structure and function. In: McLoon LK, Andrade FH, editors. Craniofacial Muscles. New York: Springer, p 207–227.

Stifani N, Freitas ARO, Liakhovitskaria A, Medvinsky A, Kania A, Stifani S. 2008. Suppression of interneuron programs and maintenance of selected spinal motor neuron fates by the transcription factor AML1/Runx1. Proc Natl Acad Sci USA 105:6451–6456.

Stifani S, Ma Q. 2009. 'Runxs and regulations' of sensory and motor neuron subtype differentiation: implications for hematopoietic development. Blood Cells Mol Dis 43:20–26.

Sturrock RR. 1991. Stability of neuron number in the subthalamic and entopeduncular nuclei of the ageing mouse brain. J Anat 179:67–73.

Takami K, Kawai Y, Shiosaka S, Lee Y, Girgis S, Hillyard CJ, MacIntyre I, Emson PC, Tohyama M. 1985. Immunohistochemical evidence for the coexistence of calcitonin gene-related peptide- and choline acetyltransferase-like immunoreactivity in neurons of the rat hypoglossal, facial and ambiguus nuclei. Brain Res 328:386–389.

Takasu N, Hashimoto PH. 1988. Morphological identification of an interneuron in the hypoglossal nucleus of the rat: a combined Golgi-electron microscopic study. J Comp Neurol 271:461–471.

Tamura S, Morikawa Y, Miyajima A, Senba E. 2003. Expression of oncostatin M receptor beta in a specific subset of nociceptive sensory neurons. Eur J Neurosci 17:2287–2298.

Terrado J, Gerrikagoitia I, Dominguez L, Raldua D, Martinez-Millan L, Sarasa M. 1999. Expression of the genes for α-type and β-type calcitonin gene-related peptide during rat embryogenesis. Neuroscience 92:713–727.

Theriault FM, Roy P, Stifani S. 2004. AML1/Runx1 is important for the development of hindbrain cholinergic branchiovisceral motor neurons and selected cranial sensory neurons. Proc Natl Acad Sci USA 101:10343–10348.

Theriault FM, Nuthall HN, Dong Z, Lo R, Barnabe-Heider F, Miller FD, Stifani S. 2005. Role for Runx1 in the proliferation and neuronal differentiation of selected progenitor cells in the mammalian nervous system. J Neurosci 25:2050–2061.

Trifonov S, Houtani T, Hamada S, Kase M, Maruyama M, Sugimoto T. 2009. In situ hybridization study of the distribution of choline acetyltransferase mRNA and its splice variants in the mouse brain and spinal cord. Neuroscience 159:344–357.

Uemura M, Takeichi M. 2006. Alpha N-catenin deficiency causes defects in axon migration and nuclear organization in restricted regions of the mouse brain. Dev Dyn 235:2559–2566.

Varela-Echavarría A, Pfaff SL, Guthrie S. 1996. Differential expression of LIM homeobox genes among motor neuron subpopulations in the developing chick brainstem. Mol Cell Neurosci 8:242–257.

Vinsant S, Mansfield C, Jimenez-Moreno R, Del Gaizo Moore V, Yoshikawa M, Hampton TG, Prevette D, Caress J, Oppenheim RW, Milligan C. 2013. Characterization of early pathogenesis in the SOD1(G93A) mouse model of ALS: part I, background and methods. Brain Behav 3:335–350.

Wang Q, Stacy T, Binder M, Marin-Padilla M, Sharpe AH, Speck NA. 1996. Disruption of the Cbfa2 gene causes necrosis and hemorrhaging in the central nervous system and blocks definitive hematopoiesis. Proc Natl Acad Sci USA 93:3444–3449.

Witzemann V. 2006. Development of the neuromuscular junction. Cell Tissue Res 326:263–271.

Wu H, Xiong WC, Mei L. 2010. To build a synapse: signaling pathways in neuromuscular junction assembly. Development 137:1017–1033.

Wu HH, Levitt P. 2013. Prenatal expression of MET receptor tyrosine kinase in the fetal mouse dorsal raphe nuclei and the visceral motor/sensory brainstem. Dev Neurosci 35:1–16.

Yamane A, Ohnuki Y, Saeki Y. 2001. Developmental changes in the nicotinic acetylcholine receptor in mouse tongue striated muscle. J Dent Res 80:1840–1844.

Yang FC, Tan T, Huang T, Christianson J, Samad OA, Liu Y, Roberson D, Davis BM, Ma Q. 2013. Genetic control of the segregation of pain-related sensory neurons innervating the cutaneous versus deep tissues. Cell Rep 5:1353–1364.

Yu T, Scully S, Yu Y, Fox GM, Jing S, Zhou R. 1998. Expression of GDNF family receptor components during development: implications in the mechanisms of interaction. J Neurosci 18:4684–4696.

Yokomizo T, Takahashi S, Mochizuki N, Kuroha T, Ema M, Wakamatsu A, Shimizu R, Ohneda O, Osato M, Okada H, Komori T, Ogawa M, Nishikawa S, Ito Y, Yamamoto M. 2007. Characterization of GATA-1(+) hemangioblastic cells in the mouse embryo. EMBO J 26:184–196.

Yoshikawa M, Senzaki K, Yokomizo T, Takahashi S, Ozaki S, Shiga T. 2007. Runx1 selectively regulates cell fate specification and axonal projections of dorsal root ganglion neurons. Dev Biol 303:663–674.

Yoshikawa M, Murakami Y, Senzaki K, Masuda T, Ozaki S, Ito Y, Shiga T. 2013. Coexpression of Runx1 and Runx3 in mechanoreceptive dorsal root ganglion neurons. Dev Neurobiol 73:469–479.

Zagami CJ, Zusso M, Stifani S. 2009. Runx transcription factors: lineage-specific regulators of neuronal precursor cell proliferation and post-mitotic neuron subtype development. J Cell Biochem 107:1063–1072.

Zhu X, Yeadon JE, Burden SJ. 1994. AML1 is expressed in skeletal muscle and is regulated by innervation. Mol Cell Biol 14:8051–8057.

FIGURE LEGENDS

Figure 1. Expression of Runx1, ChAT, CGRP, and c-Met in the wild-type hypoglossal nucleus (WT nXII). (A) Runx1 was localized in the ventrocaudal nXII in the mouse embryo. Sagittal section of nXII at E17.5 stained by anti-Runx1 antibody and thionin. (B) A schematic representation showing the region of Runx1 expression (stippled area). (C-E) Immunostaining for ChAT (C, green) and Runx1 (D, red) in WT nXII at E17.5 (frontal sections). E is the merged image of C and D. All $Runx1^{+}$ neurons expressed ChAT (E). (F-H) Immunostaining for Runx1 (F, red) and CGRP (G, green) in WT nXII at E17.5 (frontal sections). H is the merged image of F and G. Runx1 and CGRP were expressed in separate neuron populations (H). (I-K) Immunostaining for Runx1 (I, red) and c-Met (J, green) in WT nXII at E17.5 (frontal sections). K is the merged image of I and J. (L-N) Immunostaining for Runx1 (L, red) and CGRP (M, green) in WT nXII at E13.5 (sagittal sections; rostral is right and caudal is left). Runx1 and CGRP were expressed separately in most neurons (N). Arrows indicate $Runx1^{+}$ neurons. The nXIIs were outlined by the dotted lines. Scale bar: 100 μm (E,H,K,N)

Figure 2. Runx1 deficiency does not alter the expression of ChAT, CGRP, Islet-1/2, c-ret, or c-Met in the mouse nXII at E17.5. (A,B) Immunostaining for ChAT in the nXII of *Runx1*$^{+/+}$*::Tg* (A) and *Runx1*$^{-/-}$*::Tg* mice (B). A similar ChAT expression distribution was observed in both genotypes. (C,D) Immunostaining for CGRP in the nXII of *Runx1*$^{+/+}$*::Tg* (C) and *Runx1*$^{-/-}$*::Tg* mice (D). A similar CGRP expression distribution was observed. (E-J) Immunostaining for Islet-1/2 (E,H, red) and CGRP (F,I, green) in the nXII of *Runx1*$^{+/+}$*::Tg* (E-G) and *Runx1*$^{-/-}$*::Tg* mice (H-J). G and J are merged images of E and F, and H and I, respectively. (K,L) Immunostaining for c-Met in the nXII of *Runx1*$^{+/+}$*::Tg* (K) and *Runx1*$^{-/-}$*::Tg* (L). (M,N) Immunostaining for c-ret in nXII of *Runx1*$^{+/+}$*::Tg* (L) and *Runx1*$^{-/-}$*::Tg* (N). Similar Islet-1/2, c-Met, and c-ret expression patterns were observed in both genotypes, suggesting that Runx1 does not control the expression of any of these motoneuron marker proteins. The nXIIs were outlined by the dotted lines. Scale bar: 100 μm (B,D,J,L,N)

Figure 3. Runx1 deficiency disrupts axonal projection to tongue muscles and CN XII fasciculation. The expression of the axon marker neurofillament-200 (NF-H) and the motor endplate marker alpha-bungarotoxin (α-BTX) were examined in the tongue of

Runx1$^{+/+}$*::Tg* and *Runx1*$^{-/-}$*::Tg* mice at E17.5. (A-L) Sagittal (A-F) and frontal (G-L) sections of the tongue. Fewer NF-H^{+} axons were detected in tongues of *Runx1*$^{-/-}$*::Tg* mice (D) compared to *Runx1*$^{+/+}$*::Tg* mice (A). Axonal projection to the vertical (V, asterisks) and transverse (T, boxed areas, arrows) tongue muscles (A,D,G,J, green), and (α-BTX-binding) acetylcholine receptor (AChR) clusters (B,E,H,K, red), and merged images (C,F,I,L) in *Runx1*$^{+/+}$*::Tg* (A-C,G-I) and *Runx1*$^{-/-}$*::Tg* mice (D-F,J-L) at E17.5. *Runx1*$^{-/-}$*::Tg* tongue exhibited many truncated axons (J). (M-P) Expanded images of NF-H^{+} axons (green) and α-BTX^{+} AChR clusters (red) in *Runx1*$^{+/+}$*::Tg* (M,N) and *Runx1*$^{-/-}$*::Tg* (O,P) V and T muscles at E17.5. Axons appeared less tightly bundled in *Runx1*$^{-/-}$*::Tg* tongue. Scale bar: 100 μm (F,L,P)

Figure 4. Runx1 deficiency reduces the total number of tongue muscle NMJs originating from ventrocaudal hypoglossal neurons but not CGRP^{+} neurons. The area of VAChT^{+}/CGRP^{-} axon terminals but not CGRP^{+} axon terminals was reduced in *Runx1*$^{-/-}$*::Tg* tongue at E17.5. (A-F) Photomicrographs showing the expression of VAChT (A,D, green) and CGRP (B,E, red) in the anterior body of the tongue in *Runx1*$^{+/+}$*::Tg* (A-C) and *Runx1*$^{-/-}$*::Tg* mice (D-F). Sagittal sections. C and F are merged images of A and B, and D and E, respectively. (G) The area of VAChT^{+} axon terminals from all hypoglossal neurons was lower in the anterior body, posterior body, and base of the tongue in *Runx1*$^{-/-}$*::Tg* mice. (H) The area of CGRP^{+} axon terminals from Runx1^{-} neurons was unchanged in *Runx1*$^{-/-}$*::Tg* compared to *Runx1*$^{+/+}$*::Tg* mice. (I) The area of VAChT^{+}/CGRP^{-} axon terminals from Runx1^{+} neurons was significantly lower in the tongue anterior body, posterior body, and base in *Runx1*$^{-/-}$*::Tg* mice. (J) Schematic representation of hypoglossal axon terminals in the tongue. n = 3 mice for each genotype, *$p < 0.05$, #$p < 0.05$ by Student's t-test. * compared to *Runx1*$^{+/+}$*::Tg*, # compared to the anterior body of the tongue. The bars represent means ± SEM. Scale bar: 100 μm

Figure 5. Reduced numbers of NMJs but no change in the innervated fraction in V and T tongue muscles of *Runx1*$^{-/-}$*::Tg* mice at E17.5. VAChT^{+} axon terminals (A,D, green) and α-BTX^{+} AChR clusters (B,E, red) and merged images (C,F) in *Runx1*$^{+/+}$*::Tg* (A-C) and *Runx1*$^{-/-}$*::Tg* (D-F) V and T tongue muscles. (G) The number of α-BTX^{+} AChR clusters was reduced in the anterior body, posterior body, and base of *Runx1*$^{-/-}$*::Tg* V

and T tongue muscles compared to *Runx1*$^{+/+}$*::Tg*. (H) The number of α-BTX^{+} AChR clusters was reduced in the anterior body, posterior body, and base of *Runx1*$^{-/-}$*::Tg* V tongue muscle compared to *Runx1*$^{+/+}$*::Tg*. (I) The number of α-BTX^{+} AChR clusters was reduced in the anterior body, and posterior body of *Runx1*$^{-/-}$*::Tg* T tongue muscle compared to *Runx1*$^{+/+}$*::Tg*. (J) Total NMJ innervation (% of all VAChT^{+} regions expressing α-BTX^{+} AChR clusters) was not changed in *Runx1*$^{-/-}$*::Tg* V and T tongue muscles, as the number of α-BTX^{+} AChR clusters and VAChT^{+} axon terminals were decreased proportionally. $n = 3$ mice for each group, $*p < 0.05$, $**p < 0.01$ by Student's t-test. The bars represent means ± SEM. Scale bar: 100 μm

Figure 6. Increased VAChT^{+} axon terminal area in the genioglossus (GG) tongue muscle but not superior longitudinal (SL) tongue muscle in *Runx1*$^{-/-}$*::Tg* mice at E17.5. VAChT^{+} axon terminals (A,D, green) and α-BTX^{+} AChR clusters (B,E, red) and merged images (C,F) in *Runx1*$^{+/+}$*::Tg* (A-C) and *Runx1*$^{-/-}$*::Tg* (D-F) GG tongue muscles at E17.5. (G) The area of VAChT^{+} axon terminals was significantly increased in *Runx1*$^{-/-}$*::Tg* GG muscle. (H) The area of VAChT^{+} axon terminals was not changed in *Runx1*$^{-/-}$*::Tg* SL tongue muscle. (I) The percentage of NMJ innervation was not changed in *Runx1*$^{-/-}$*::Tg* GG tongue muscle. (J) The number of AChR clusters was not changed in *Runx1*$^{-/-}$*::Tg* GG tongue muscle. $n = 3$ mice for each group, $*p < 0.05$ as determined by Student's t-test. The bars represent means ± SEM. Scale bar: 25 μm

Figure 7. Runx1 deficiency does not result in ectopic innervation of other tongue muscles. Similar distribution of hypoglossal neurons labeled retrogradely from GG tongue muscle tracer injection in *Runx1*$^{+/+}$*::Tg* and *Runx1*$^{-/-}$*::Tg* mice. (A-F) The distribution of retrogradely labeled hypoglossal neurons in the ventrocaudal nXII of *Runx1*$^{+/+}$*::Tg* (A-C) and *Runx1*$^{-/-}$*::Tg* mice (D-F) at E17.5. Cholera toxin B subunit (CTB) was injected into GG tongue muscle for retrograde labeling of hypoglossal neurons (A,D, red). CGRP^{+} hypoglossal neurons (B,E, green) and merged images of A and B (C) and D and E (F). Many CGRP^{+} CTB-labeled hypoglossal neurons were observed in both *Runx1*$^{+/+}$*::Tg* (C) and *Runx1*$^{-/-}$*::Tg* mice (F), indicating that a Runx1 deficit did not substantially alter axonal projections to the GG muscle. The dorsal and ventral regions were outlined by the dotted lines. $n = 4$ mice for each group. Scale bar: 50 μm

Figure 8. Reduced expression of Fzd3 in the nXII of *Runx1*$^{-/-}$*::Tg* mice at E17.5. (A-F) Immunostaining for Fzd3 (A,D, green) and Islet-1/2 (B,E, red) and merged images (C,F) in *Runx1*$^{+/+}$*::Tg* (A-C) and *Runx1*$^{-/-}$*::Tg* mice (D-F). (G) Fzd3 expression was lower in hypoglossal neurons of *Runx1*$^{-/-}$*::Tg* compared to *Runx1*$^{+/+}$*::Tg* mice. The nXIIs were outlined by the dotted lines. n = 3 mice for each group, *$p < 0.005$ as determined by Student's t-test. The bars represent means ± SEM. Scale bar: 100 μm

Figure 9. Runx1 deficiency did not induce tongue muscle abnormalities. (A) The expression of Runx1 in the tongue of WT mice at E17.5. Runx1 was expressed in the dermal papillae (arrows) but not in tongue muscle tissue. (B-G) Immunostaining for myosin (B,E, green) and α-BTX (C,F, red), and merged images (D,G) of the tongue in *Runx1*$^{+/+}$*::Tg* (B-D) and *Runx1*$^{-/-}$*::Tg* mice (E-G) at E17.5. There were no demonstrable changes in myosin and α-BTX distribution or immunostaining intensity. Vs and Ts indicate the vertical and transverse tongue muscles, respectively. Scale bar: 100 μm (A,G)

Supplemental Figure 1. Myotopy of the axonal projection from nXII to the tongue. (A) Schematic representation showing frontal sections of nXII from rostral to caudal. The left half shows the compartments of nXII and associated nerve branches. The nXII is divided into two major compartments, a dorsal division (Dd) and a ventral division (Vd), the axons of which from the lateral branch (Lbr) and medial branch (Mbr) of the hypoglossal nerve, respectively. The right half shows the locations of motoneurons that innervate the genioglossus (GG), hypoglossus (HY), inferior longitudinal (IL), superior longitudinal (SL), styloglossus (STY), transverse (T), and vertical (V) tongue muscles. (B) The distribution of axon terminals in the core region of the tongue. The body and the base of tongue are innervated by motoneurons in the caudal and rostral parts of the ventral nXII, respectively. These figures are reconstructed according to Aldes (1995). (C) The distribution of retrogradely labeled hypoglossal neurons in the ventrocaudal nXII at E17.5 in WT mice. CTB was injected into the extrinsic GG tongue muscle (red) and intrinsic V and T tongue muscles (green) to label projecting hypoglossal neurons. Scale bar: 50 μm

Supplemental Figure 2. Method for measurement of axon terminal area in the tongue muscles of *Runx1*$^{+/+}$*::Tg* and *Runx1*$^{-/-}$*::Tg* mice. We took six images from sagittal sections spanning from the tip to the base of the tongue. Boxes 1 and 2, 3 and 4, and 5 and 6 correspond to the anterior body, the posterior body, and the base of the tongue, respectively. Total areas of VAChT^{+} axon terminals in box 1 (200 × 200 μm; a, a') and in boxes 2–6 (200 × 600 μm; b, b') were measured, revealing a reduced axon terminal density in the tongue muscles of *Runx1*$^{-/-}$*::Tg* mice.

Supplemental Figure 3. Effects of Runx1 deficiency on axonal projection to tongue muscles. (A,B) The expression of the axon marker neurofillament-200 (NF-H) was examined in the tongue of *Runx1*$^{+/+}$*::Tg* and *Runx1*$^{-/-}$*::Tg* mice at E13.5. Fewer NF-H^{+} axons were detected in tongues of *Runx1*$^{-/-}$*::Tg* mice (B) compared to *Runx1*$^{+/+}$*::Tg* mice (A) at E13.5. (C-H) The expression of the axon terminal marker VAChT and the motor endplate marker alpha-bungarotoxin (α-BTX) was examined in the tongue of *Runx1*$^{+/+}$*::Tg* and *Runx1*$^{-/-}$*::Tg* mice at E15.5. VAChT^{+} axon terminals (C,F, green) and (α-BTX-binding) acetylcholine receptor (AChR) clusters (D,G, red) and merged images (E,H) in *Runx1*$^{+/+}$*::Tg* (C-E) and *Runx1*$^{-/-}$*::Tg* (F-H) tongue muscles. Only α-BTX expression (denervated neuromuscular junction, boxed areas) were observed frequently in *Runx1*$^{-/-}$*::Tg* tongue muscles. Scale bar: 100 μm (B,H)

Fig.1

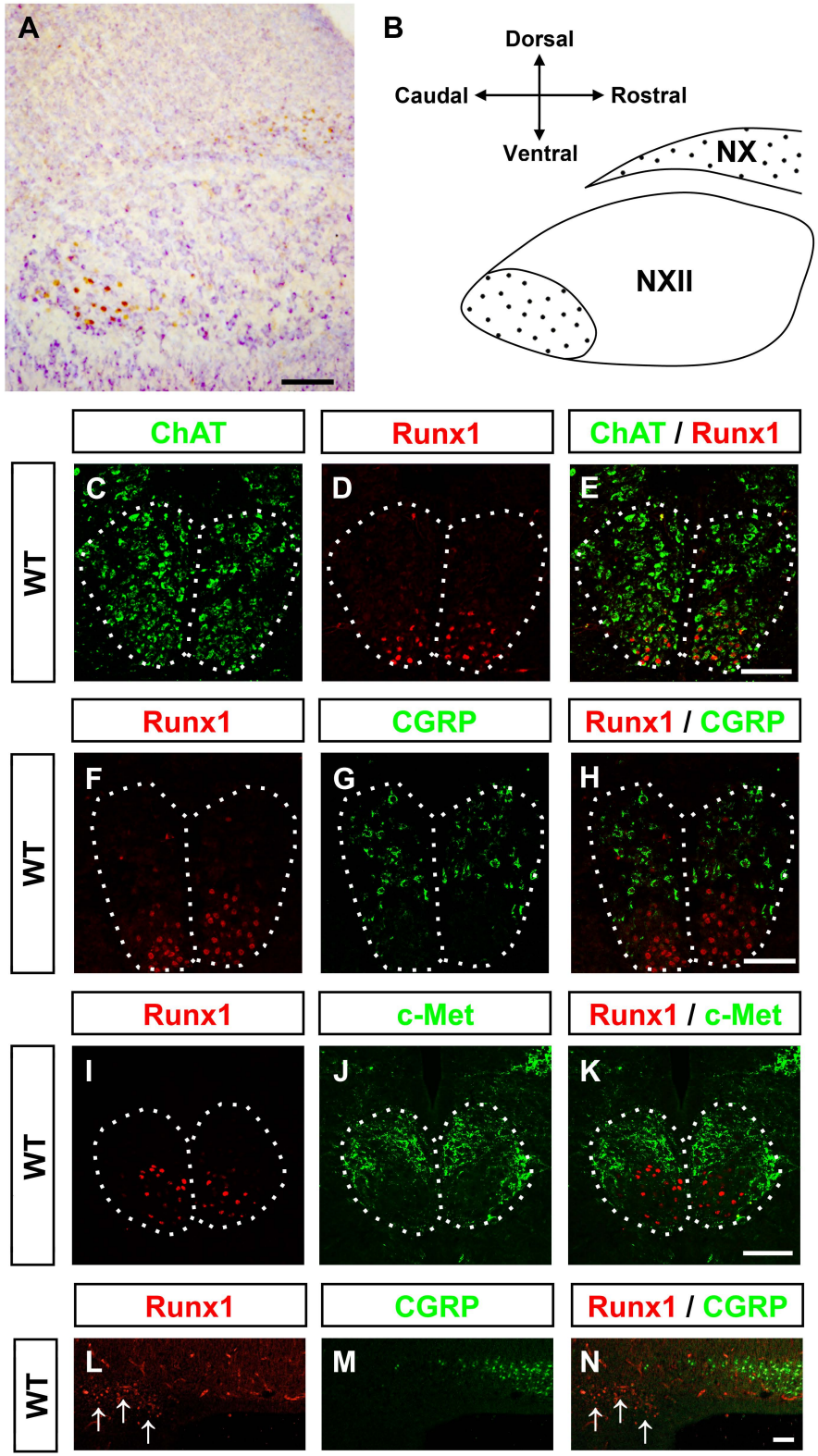
A
B
Dorsal
Caudal
Rostral
Ventral
NX
NXII
ChAT
Runx1
ChAT / Runx1
WT
C
D
E
Runx1
CGRP
Runx1 / CGRP
F
G
H
Runx1
c-Met
Runx1 / c-Met
I
J
K
Runx1
CGRP
Runx1 / CGRP
L
M
N

Fig.2

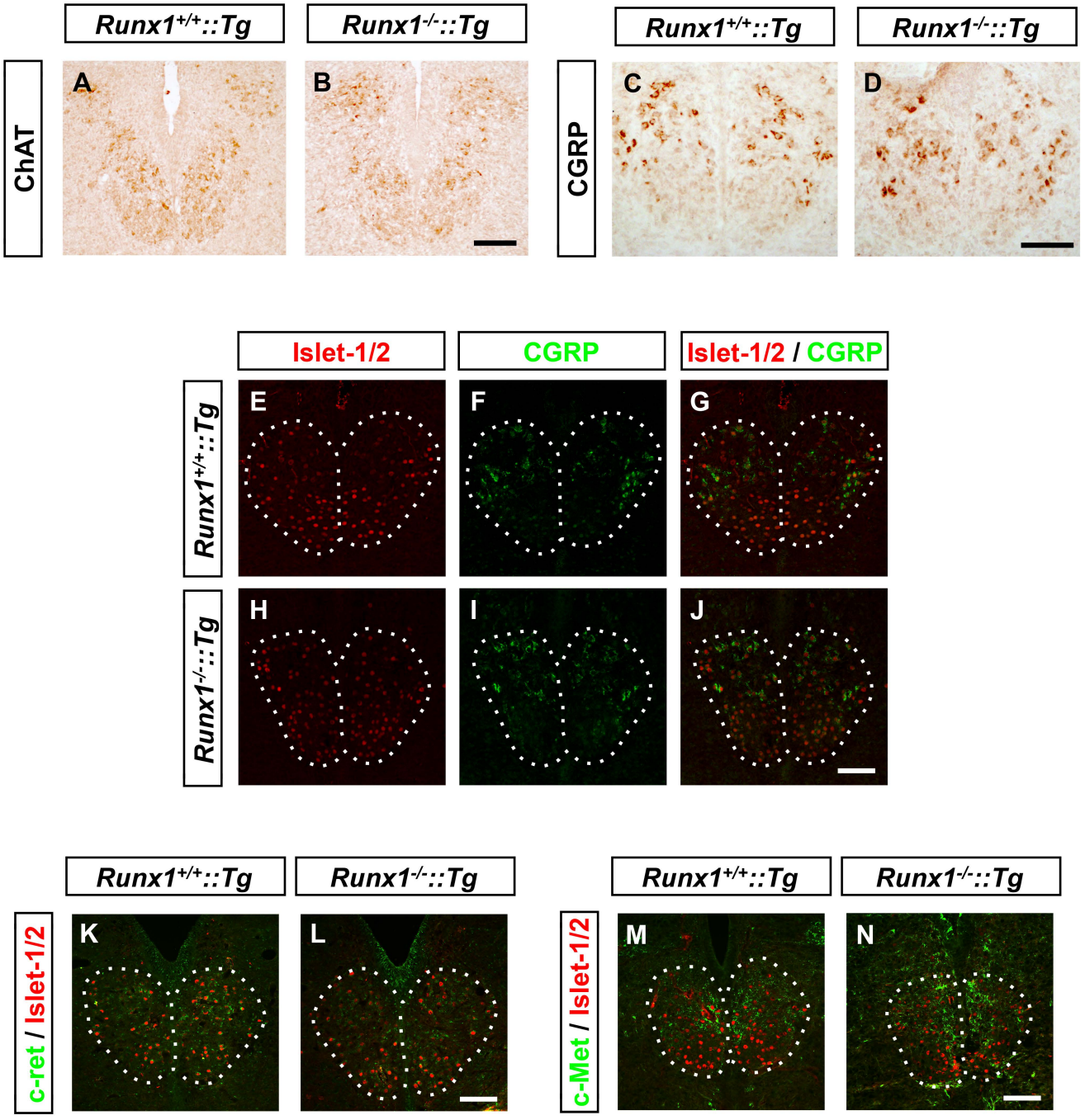
Runx1+/+::Tg
Runx1-/-::Tg
ChAT
A
B
CGRP
C
D
Islet-1/2
CGRP
Islet-1/2 / CGRP
E
F
G
H
I
J
c-ret / Islet-1/2
K
L
c-Met / Islet-1/2
M
N

Fig.3

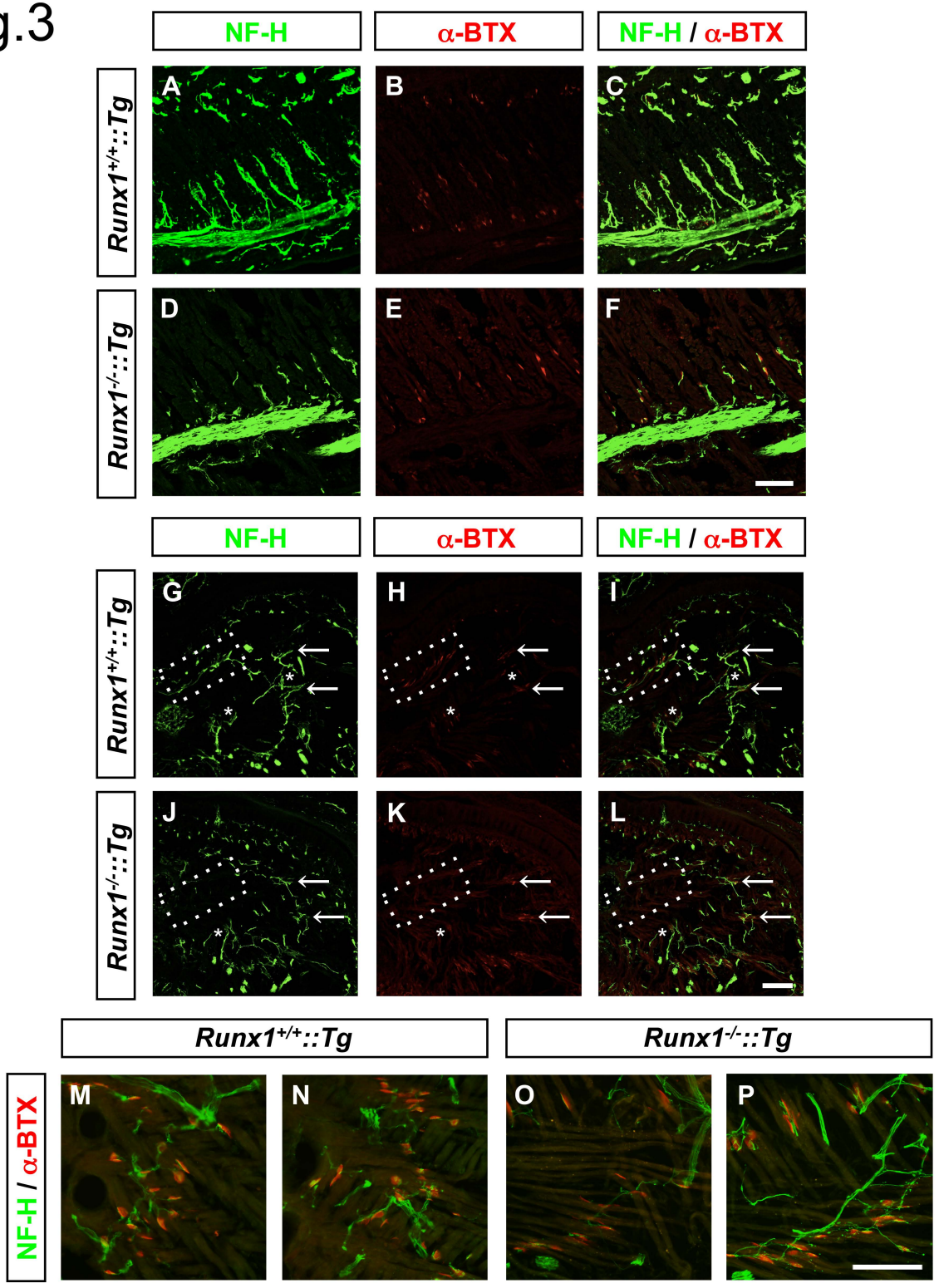

Fig.4

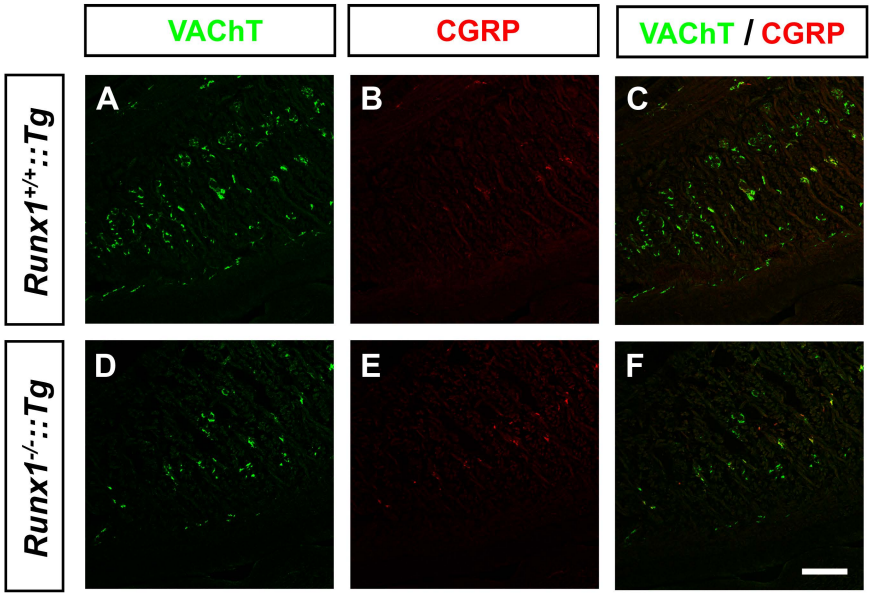
VAChT
CGRP
VAChT / CGRP
Runx1+/+::Tg
Runx1-/-::Tg
A
B
C
D
E
F

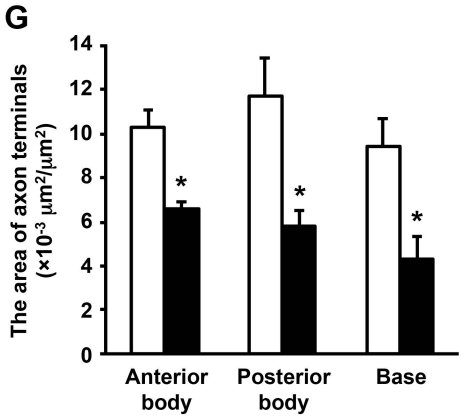
G
The area of axon terminals (×10-3 μm2/μm2)
Anterior body
Posterior body
Base

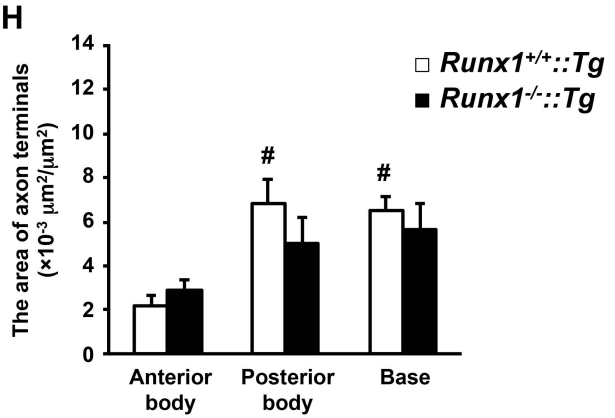
H
Runx1+/+::Tg
Runx1-/-::Tg
The area of axon terminals (×10-3 μm2/μm2)
Anterior body
Posterior body
Base

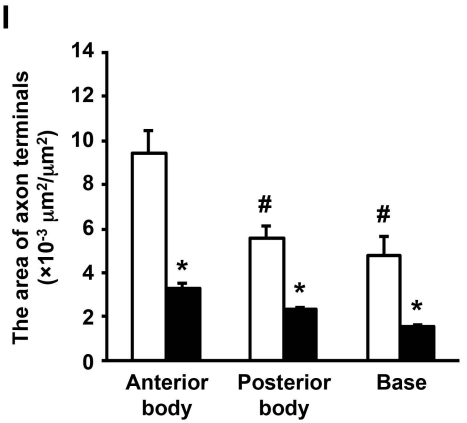
I
The area of axon terminals (×10-3 μm2/μm2)
Anterior body
Posterior body
Base

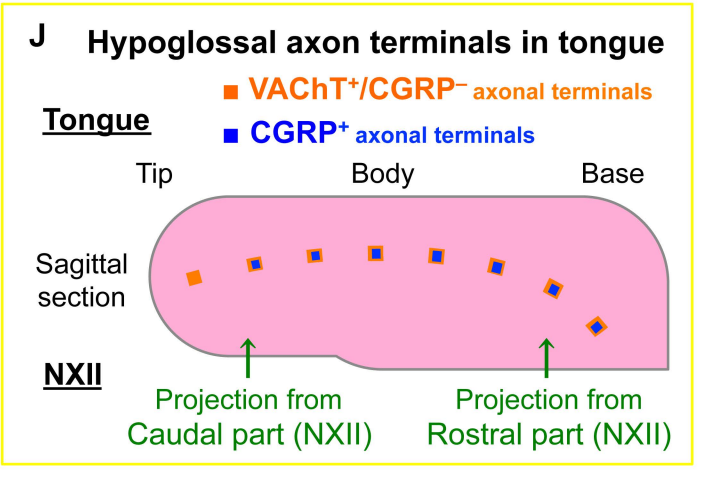
J
Hypoglossal axon terminals in tongue
VAChT+/CGRP− axonal terminals
CGRP+ axonal terminals
Tongue
Tip
Body
Base
Sagittal section
NXII
Projection from Caudal part (NXII)
Projection from Rostral part (NXII)

Fig.5

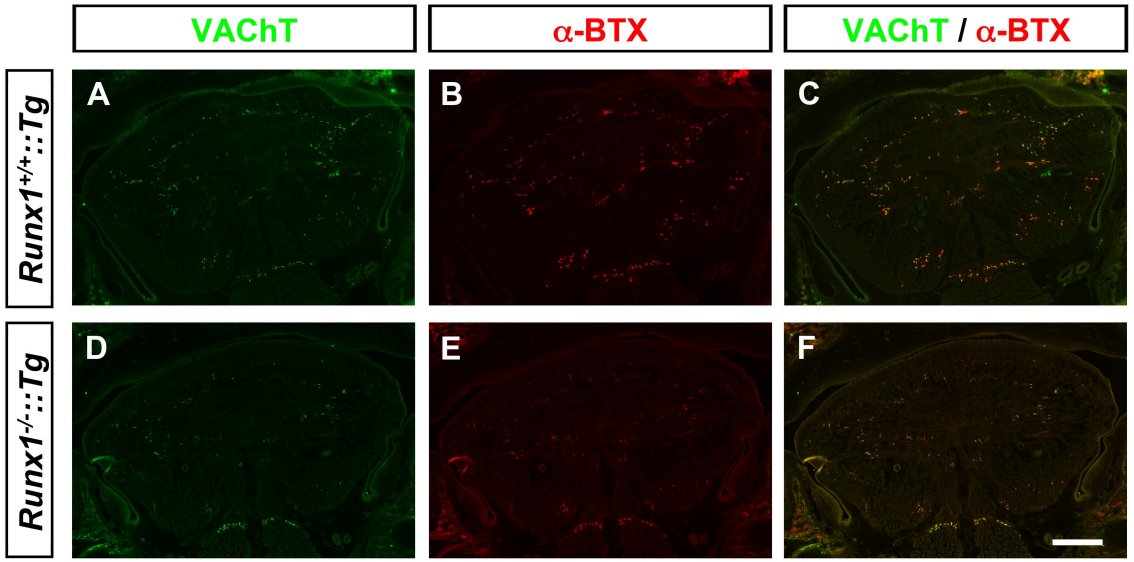
VAChT
α-BTX
VAChT / α-BTX
Runx1+/+::Tg
Runx1-/-::Tg
A
B
C
D
E
F

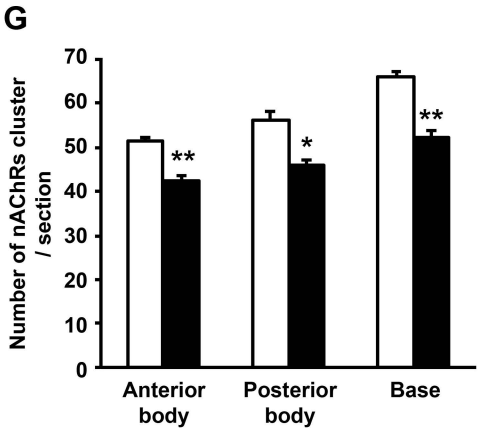
G
Number of nAChRs cluster / section
70
60
50
40
30
20
10
0
**
*
**
Anterior body
Posterior body
Base

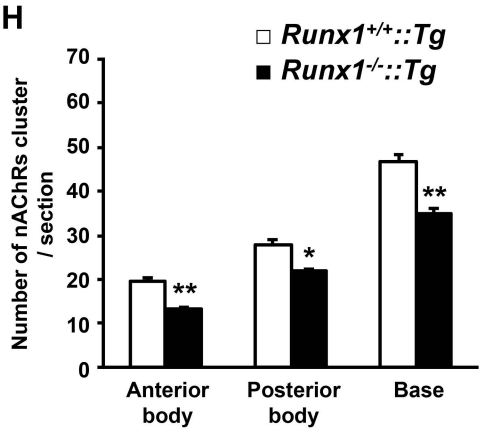
H
□ Runx1+/+::Tg
■ Runx1-/-::Tg
Number of nAChRs cluster / section
70
60
50
40
30
20
10
0
**
*
**
Anterior body
Posterior body
Base

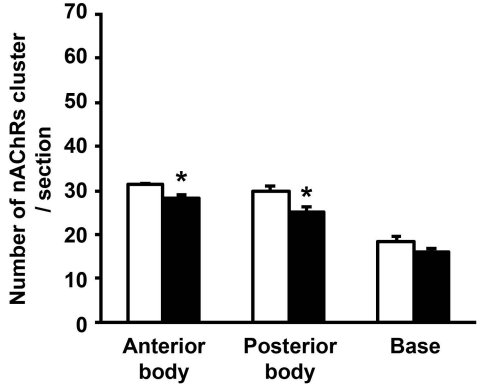
I
Number of nAChRs cluster / section
70
60
50
40
30
20
10
0
*
*
Anterior body
Posterior body
Base

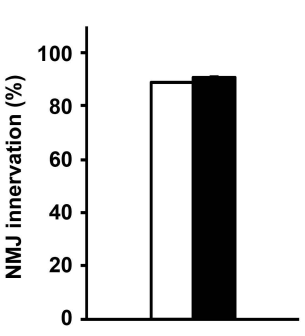
J
NMJ innervation (%)
100
80
60
40
20
0

Fig.6

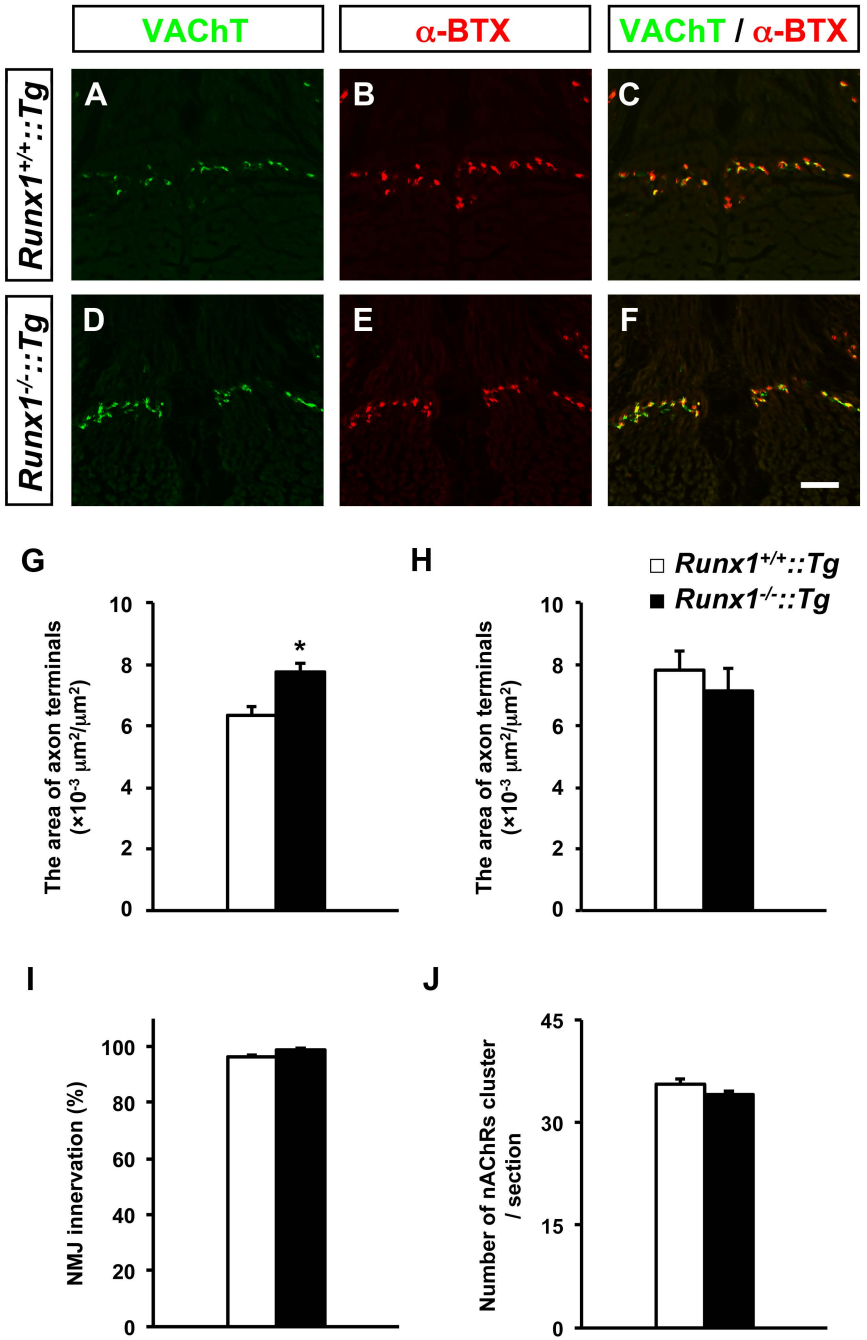
VAChT
α-BTX
VAChT / α-BTX
Runx1+/+::Tg
Runx1-/-::Tg
A
B
C
D
E
F
G
H
□ Runx1+/+::Tg
■ Runx1-/-::Tg
The area of axon terminals (×10-3 μm2/μm2)
*
I
NMJ innervation (%)
J
Number of nAChRs cluster / section

Fig.7

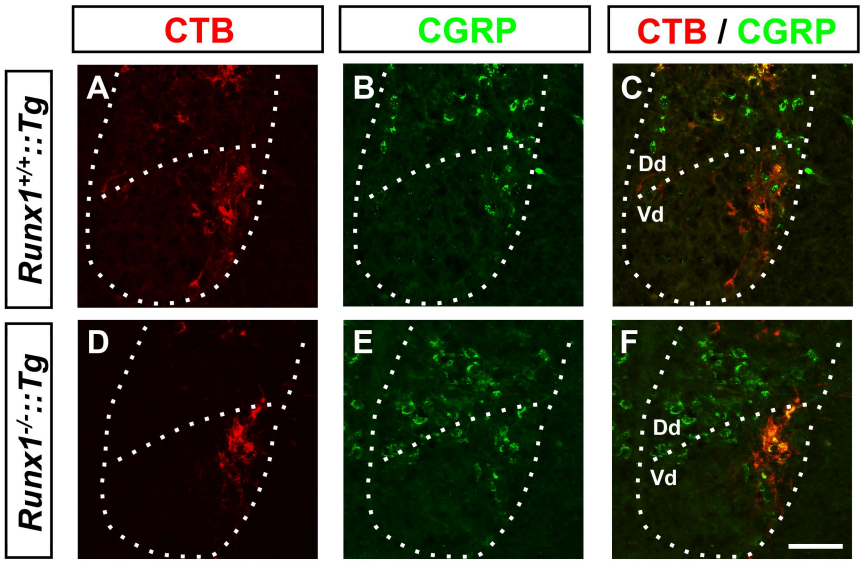

Fig.8

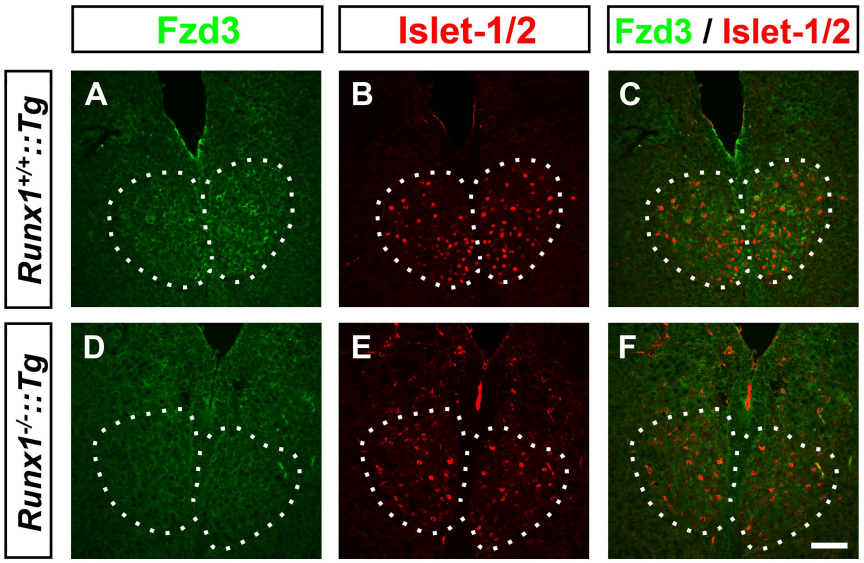
Fzd3
Islet-1/2
Fzd3 / Islet-1/2
Runx1+/+::Tg
Runx1-/-::Tg
A
B
C
D
E
F

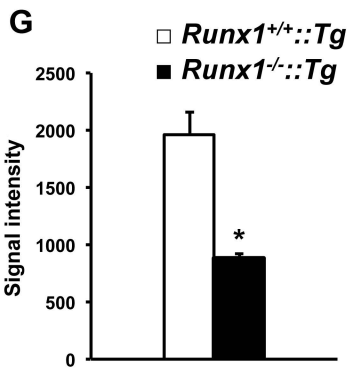
G
Runx1+/+::Tg
Runx1-/-::Tg
Signal intensity
2500
2000
1500
1000
500
0
*

Fig.9

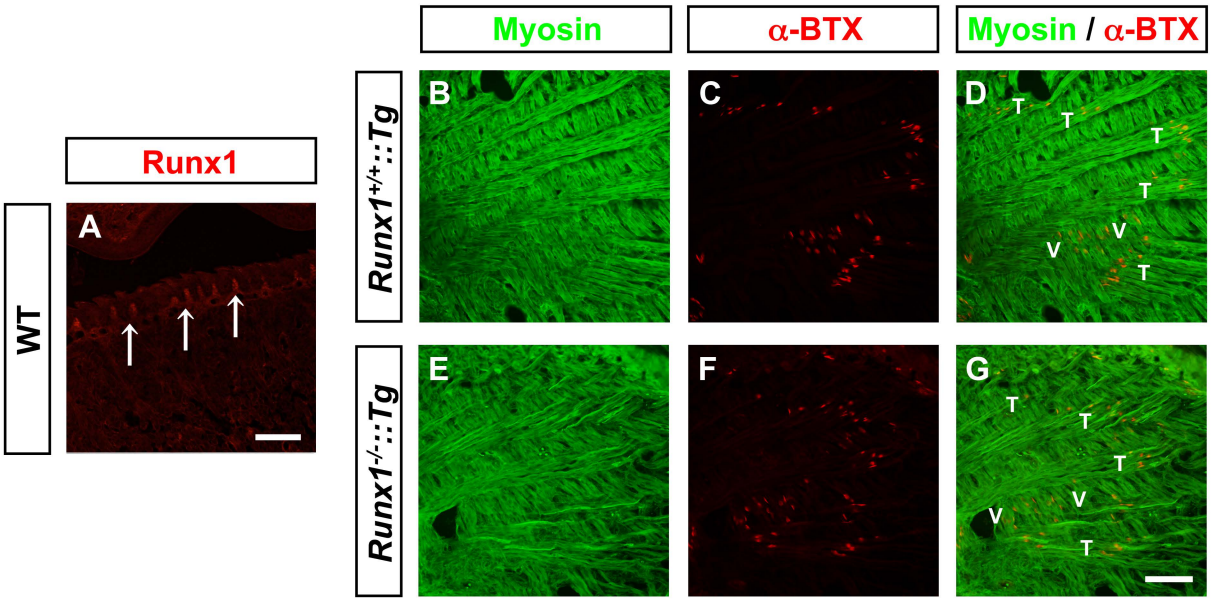
Runx1
WT
A
Myosin
α-BTX
Myosin / α-BTX
Runx1+/+::Tg
Runx1-/-::Tg
B
C
D
E
F
G
T
V

Fig.S1

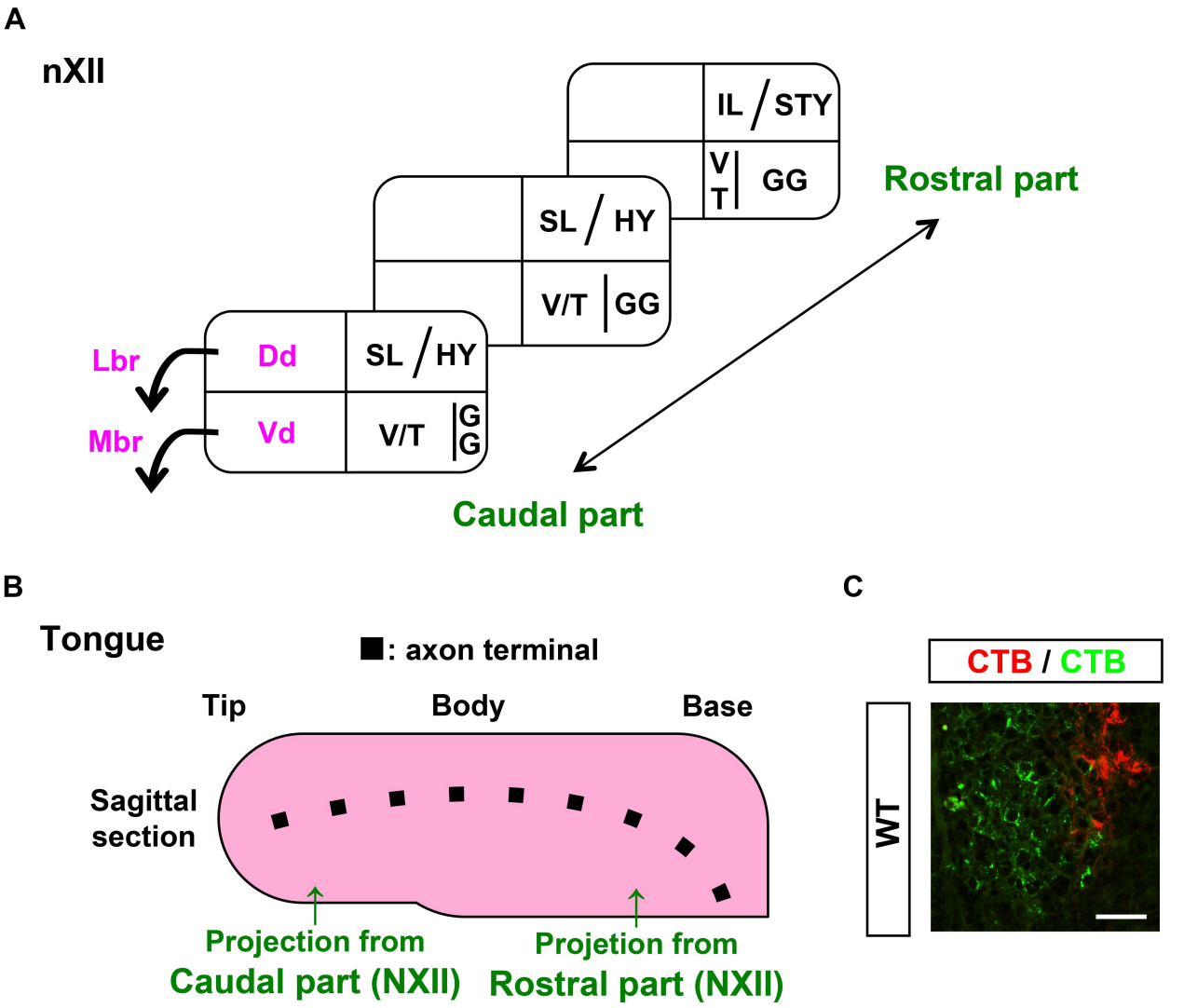
A
nXII
IL / STY
V
T
GG
SL / HY
V/T
GG
Dd
SL / HY
Vd
V/T
G
G
Lbr
Mbr
Rostral part
Caudal part
B
Tongue
■: axon terminal
Tip
Body
Base
Sagittal section
Projection from Caudal part (NXII)
Projetion from Rostral part (NXII)
C
CTB / CTB
WT

Fig.S2

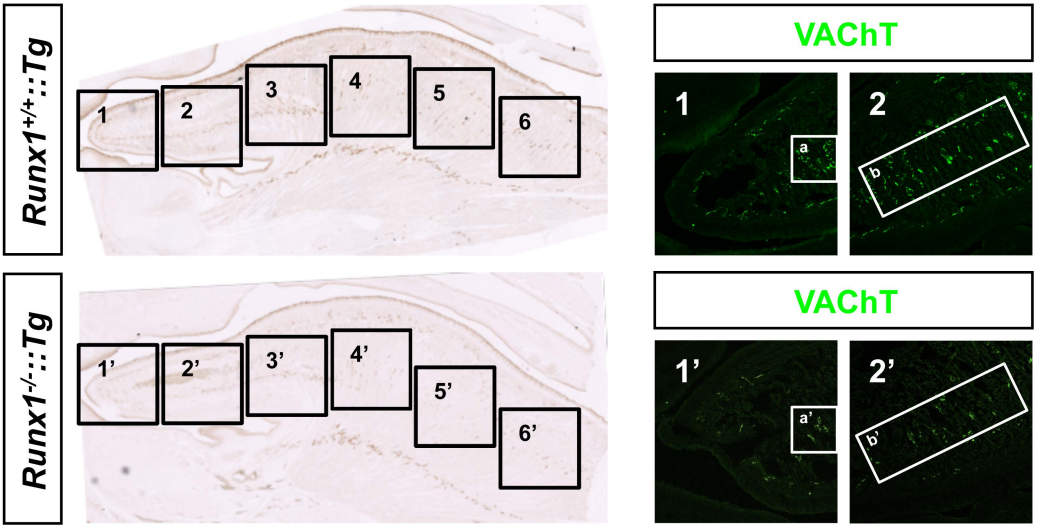

Fig.S3

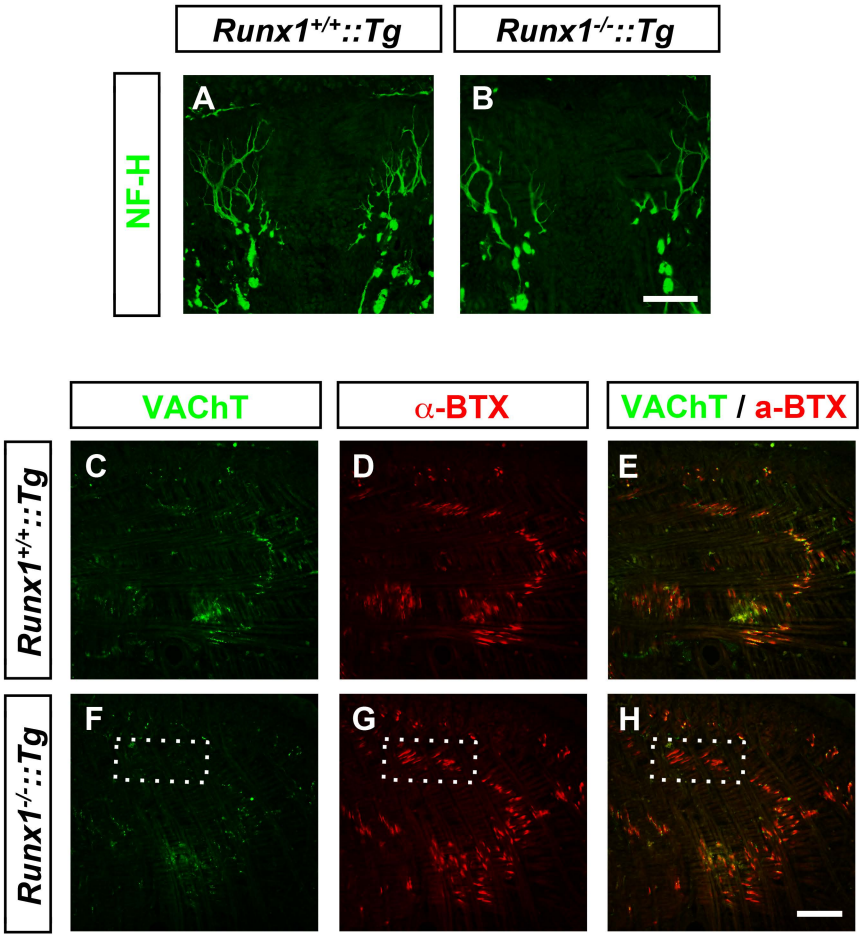
Runx1+/+::Tg
Runx1-/-::Tg
NF-H
A
B
VAChT
α-BTX
VAChT / a-BTX
Runx1+/+::Tg
Runx1-/-::Tg
C
D
E
F
G
H